

Galaxy Evolution in Cosmological Simulations with Outflows II: Metallicities and Gas Fractions

Romeel Davé¹, Kristian Finlator², Benjamin D. Oppenheimer³

¹ *Astronomy Department, University of Arizona, Tucson, AZ 85721, USA*

² *Hubble Fellow; Physics Department, University of California, Santa Barbara, CA 93106, USA*

³ *Leiden Observatory, Leiden University, PO Box 9513, 2300 RA Leiden, Netherlands*

20 August 2019

ABSTRACT

We use cosmological hydrodynamic simulations to investigate how inflows, star formation, and outflows govern the the gaseous and metal content of galaxies within a hierarchical structure formation context. In our simulations, galaxy metallicities are established by a balance between inflows and outflows as governed by the mass outflow rate, implying that the mass-metallicity relation reflects how the outflow rate varies with stellar mass. Gas content, meanwhile, is set by a competition between inflow into and gas consumption within the interstellar medium, the latter being governed by the star formation law, while the former is impacted by both wind recycling and preventive feedback. Stochastic variations in the inflow rate move galaxies off the equilibrium mass-metallicity and mass-gas fraction relations in a manner correlated with star formation rate, and the scatter is set by the timescale to re-equilibrate. The evolution of both relations from $z = 3 \rightarrow 0$ is slow, as individual galaxies tend to evolve mostly along the relations. Gas fractions at a given stellar mass slowly decrease with time because the cosmic inflow rate diminishes faster than the consumption rate, while metallicities slowly increase as infalling gas becomes more enriched. Observations from $z \sim 3 \rightarrow 0$ are better matched by simulations employing momentum-driven wind scalings rather than constant wind speeds, but all models predict too low gas fractions at low masses and too high metallicities at high masses. All our models reproduce observed second-parameter trends of the mass-metallicity relation with star formation rate and environment, indicating that these are a consequence of equilibrium and not feedback. Overall, the analytical framework of our equilibrium scenario broadly captures the relevant physics establishing the galaxy gas and metal content in simulations, which suggests that the cycle of baryonic inflows and outflows centrally governs the cosmic evolution of these properties in typical star-forming galaxies.

1 INTRODUCTION

Galaxies’ stellar, gas, and metal content determine the majority of their observable properties across all wavelengths. Hence understanding the co-evolution of these basic constituents is at the heart of developing a comprehensive theory for the formation and evolution of galaxies. Advancing observations have now characterised these properties in galaxies back into the peak epoch of cosmic star formation and beyond. Such observations provide stringent tests for galaxy formation models, and offer new opportunities to constrain the physical processes that govern galaxy evolution.

Observations have revealed tight correlations between stars, gas, and metals in galaxies. One example is the relationship between stellar mass (M_*) and star formation rate (SFR), called the main sequence for star-forming galaxies (Noeske et al. 2007); it is slightly sub-linear and evolves with redshift roughly independently of mass (Elbaz et al.

2007; Daddi et al. 2007; Davé 2008). Another example is the correlation between stellar mass and gas-phase metallicity, called the mass-metallicity relation (MZR; e.g. Tremonti et al. 2004), which shows a remarkably low scatter across a wide range in mass (Lee et al. 2006). Moreover, departures from the mean relation are strongly correlated with other galaxy properties (Ellison et al. 2008; Cooper et al. 2008; Peebles, Pogge, & Stanek 2009; Mannucci et al. 2010). The scatter in metallicity is tightest when correlated with stellar mass (Tremonti et al. 2004), suggesting that stellar mass is primarily responsible for governing the metal content of galaxies. The gas content is more difficult to measure because all phases must be accounted for (atomic, molecular, and ionised), but still shows a fairly tight anti-correlation with stellar mass (Catinella et al. 2010; Peebles & Shankar 2010). These relations evolve with redshift, towards lower metallicity (Savaglio et al. 2005; Erb et al. 2006; Zahid, Kewley, & Bresolin 2010) and higher

gas content (Erb et al. 2006b; Tacconi et al. 2010) at higher redshift.

These trends are qualitatively consistent with the canonical scenario for galaxy formation in which galaxies start out with a gaseous halo that cools onto a central disk, forms stars, and self-enriches while consuming its gas (e.g. Rees & Ostriker 1977; White & Rees 1978). However, more detailed observations have shown that the gas consumption rates would exhaust the gas supply quickly, and therefore continual replenishment of gas appears to be required to sustain star formation (Tacconi et al. 2010; Genzel et al. 2010; Papovich et al. 2010). Moreover, the metallicity evolution is quite slow, straining self-enrichment models (e.g. the classical G-dwarf problem). Hierarchical structure formation generically predicts inflow and merging that spur galaxy growth. But unfettered inflow grossly overproduces global star formation, known as the overcooling problem (e.g. Davé et al. 2001; Balogh et al. 2001). Therefore feedback processes must strongly regulate galaxy growth. Such feedback processes are expected to manifest themselves in the evolution of the mass, metal, and gaseous content of galaxies. Hence understanding the origin and evolution of scaling relations between these constituents provides key insights into accretion and feedback processes that govern galaxy growth.

Cosmological hydrodynamic simulations have advanced rapidly over the past decade, to a point where they can plausibly match a wide range of properties of galaxies and the intergalactic medium (IGM) across cosmic time. One recently-explored physical process that greatly improves concordance with observations is strong and ubiquitous galactic outflows. These outflows are powered by supernovae, stellar winds, and/or photons from young stars, i.e. they result from the star formation process itself, leading to self-regulated growth. Qualitatively, observations indicate that galaxy formation must be increasingly suppressed towards small masses. Outflows are now directly observed in most star-forming galaxies at $z \gtrsim 1$ (e.g. Weiner et al. 2009; Steidel et al. 2010). By incorporating outflows as observed into simulations, it is possible to yield galaxy populations that significantly more closely resemble those observed.

Recently, it has been found that simulations employing outflow scalings as expected for momentum-driven winds (Murray, Quataert, & Thompson 2005; Zhang & Thompson 2010) are among the most successful at matching a wide range of data on galaxies (e.g. Davé, Finlator, & Oppenheimer 2006; Finlator & Davé 2008; Oppenheimer et al. 2010) and the IGM (e.g. Oppenheimer & Davé 2006, 2008, 2009; Oppenheimer, Davé, & Finlator 2009), although notable discrepancies remain. These scalings assume that the mass outflow rate scales inversely with galaxy circular velocity, providing increased suppression of star formation in smaller systems. Such outflows also have interesting unanticipated consequences. For instance, Oppenheimer & Davé (2008) found that ejected wind material more often than not returned into galaxies, and that this so-called wind recycling accretion becomes stronger at higher masses and dominates the global accretion onto galaxies at $z \lesssim 1$ (Oppenheimer et al. 2010). Furthermore, winds also have a “preventive” feedback effect particularly in smaller galaxies, by adding energy to surrounding gas which

curtails inflow into the interstellar medium of galaxies relative to inflow into the halo (Oppenheimer et al. 2010; van de Voort et al. 2010; Faucher-Giguere, Kereš, & Ma 2011). The high outflow rates and frequent re-accretion suggest a continual cycling of baryons between galaxies and their surrounding IGM, and that this cycle is responsible for governing the observable properties of both.

In this series of two papers, we investigate the way in which inflows and outflows within a hierarchical structure formation context govern the main constituents of galaxies, namely stars, gas, and metals. In Davé, Oppenheimer, & Finlator (2011, hereafter Paper I) we focused on stellar masses and star formation rates. We argue that many of the trends seen in simulations can be understood within the framework of galaxies living in a slowly-evolving equilibrium between inflow, outflow, and star formation. The inflow is at early epochs supplied primarily from the (relatively) pristine IGM, while at later times wind recycling brings back gas in a mass-dependent fashion. As in Oppenheimer et al. (2010), we showed that outflows produce three-tiered stellar mass and star formation rate functions, where the middle tier is established by the onset of differential (i.e. mass-dependent) wind recycling. The evolution and mass dependence of the specific star formation follows trends arising from the mass accretion rate into halos, modulated by outflows. We further examined the satellite galaxy population, and found that in models they are not particularly more common or more bursty than central galaxies at a given mass, and that the main difference versus centrals is that satellites have increasingly suppressed star formation to small masses. We showed that momentum-driven wind scalings provide the best overall fit to available observations, but the agreement is only good in the range of $\sim (0.1 - 1)L^*$. At lower masses, star formation in dwarfs seems to occur at too early epochs in the models, and at higher masses some additional mechanism is required to quench star formation in massive galaxies (e.g. black hole feedback; Gabor et al. 2011). Overall, comparing these simulations to observations helps constrain the way in which inflows and outflows work together to govern the growth of galaxies’ stellar component, while highlighting key failures of current models.

In this paper, Paper II in this series, we extend the analysis of our suite of cosmological hydrodynamic simulations with outflows to examine galaxy metallicities and gas fractions. The primary goal is to understand how outflows govern scaling relations between these quantities and their stellar content. We will show that the equilibrium scenario introduced in Paper I also provides the basic intuition for understanding gas and metal growth. We outline a simple analytic formalism that captures the main features of the simulation results. In it, the metallicity of galaxies is governed primarily by outflows with a secondary effect from enriched infall, while the gas content is governed by a competition between cosmological gas supply and the gas consumption rate set by the star formation law. Both the metallicity and gas fraction are driven by cosmic inflows, which diminish rapidly with cosmic time, and fluctuate on shorter timescales resulting in deviations from the mean relations that correlate with star formation. By comparing to observations we find that the momentum-driven wind scalings provide the best match to data among the models examined here, but once again there are significant discrepancies at

the highest and lowest masses. These results highlight how galactic outflows are a key moderator of the stellar, metal, and gas content of galaxies at all epochs, and in turn observations of these properties provide valuable insights into the cosmic ecosystem within which galaxies form and grow.

The paper is organized as follows. In §2 we briefly describe our hydrodynamic simulations including our galactic outflow models. In §3 we examine simulated mass-metallicity relations across cosmic time, and present a simple framework for understanding their physical origin. In §4 we similarly examine galaxy gas fractions. In §5 we compare to observations of metal and gas content to identify broad constraints on feedback processes. In §6 we discuss second-parameter dependences of the MZR and gas fractions with star formation rate and environment. In §7 we explore how individual galaxies evolve in the mass-metallicity and mass-gas fraction planes. Finally, we summarize and discuss the broader implications of our work in §8.

2 SIMULATIONS

The suite of simulations employed are identical to that in Paper I. We refer the reader there for a full discussion of all details, and here briefly review some of the key aspects.

2.1 Runs

Our simulations are run with an extended version of the GADGET-2 N-body + Smoothed Particle Hydrodynamic (SPH) code (Springel 2005). We assume a Λ CDM cosmology (Hinshaw et al. 2009): $\Omega_M = 0.28$, $\Omega_\Lambda = 0.72$, $h \equiv H_0/(100 \text{ km s}^{-1} \text{ Mpc}^{-1}) = 0.7$, a primordial power spectrum index $n = 0.96$, an amplitude of the mass fluctuations scaled to $\sigma_8 = 0.82$, and $\Omega_b = 0.046$. We call this the r-series, where our general naming convention is $r[\text{boxsize}]n[\text{particles/side}][\text{wind model}]$. Our primary runs use a boxsize of $48h^{-1}\text{Mpc}$ on a side with 384^3 dark matter and 384^3 gas particles, and a softening length of $\epsilon = 2.5h^{-1}\text{kpc}$ (comoving, Plummer equivalent). To expand our dynamic range we run two additional sets of simulations with 2×256^3 particles identical to the primary runs, except one having a boxsize of $24h^{-1}\text{Mpc}$ and $\epsilon = 1.875h^{-1}\text{kpc}$, and the other with a boxsize of $48h^{-1}\text{Mpc}$ and $\epsilon = 3.75h^{-1}\text{kpc}$. SPH particle masses are $3.6 \times 10^7 M_\odot$, $1.5 \times 10^7 M_\odot$, and $12 \times 10^7 M_\odot$ for the r48n384, r24n256, and r48n256 series, respectively, and dark matter particles masses are approximately $5 \times$ larger.

Our version of GADGET-2 includes cooling processes using the primordial abundances as described in Katz et al. (1996) and metal-line cooling as described in Oppenheimer & Davé (2006). Star formation is modeled using a subgrid recipe introduced in Springel & Hernquist (2003) where a gas particle above a density threshold of $n_H = 0.13 \text{ cm}^{-3}$ is modeled as a fraction of cold clouds embedded in a warm ionized medium following McKee & Ostriker (1977). Star formation (SF) follows a Schmidt law (Schmidt 1959) with the SF timescale scaled to match the $z = 0$ Kennicutt law (Kennicutt 1998). We use a Chabrier (2003) initial mass function (IMF) throughout. We account for metal enrichment from Type II supernovae (SNe), Type Ia SNe, and AGB stars, and we

track four elements (C,O,Si,Fe) individually, as described in Oppenheimer & Davé (2008).

Galactic outflows are implemented using a Monte Carlo approach analogous to star formation. Outflows are directly tied to the SFR, using the relation $\dot{M}_{\text{wind}} = \eta \dot{M}_{\text{SF}}$, where η is defined as the mass loading factor. The probabilities for a gas particle to spawn a star particle are calculated from the subgrid model described above, and the probability to be launched in a wind is η times that. If the particle is selected to be launched, it is given an additional velocity of v_w in the direction of $\mathbf{v} \times \mathbf{a}$, where \mathbf{v} and \mathbf{a} are the particle's instantaneous velocity and acceleration, respectively. Choices of the parameters η and v_w define the “wind model”. Once a gas particle is launched, its hydrodynamic (not gravitational) forces are turned off until either $1.95 \times 10^{10}/(v_w (\text{km s}^{-1}))$ years have passed or, more often, the gas particle has reached 10% of the SF critical density. This attempts to mock up chimneys generated by outflows that allow relatively unfettered escape from the galactic ISM, and which are not properly captured by the spherically-averaging SPH algorithm at $\gtrsim \text{kpc}$ resolution; it also yields results that are less sensitive to numerical resolution (Springel & Hernquist 2003b). For a further discussion of hydrodynamic decoupling, see Dalla Vecchia & Schaye (2008) and Paper I.

For this paper we run four wind models:

- (i) **No winds (nw)**, where we do not include outflows (i.e. $\eta = 0$);
- (ii) **Constant winds (cw)**, where $\eta = 2$ and $v_w = 680 \text{ km s}^{-1}$ for all galaxies;
- (iii) **Slow winds (sw)**, where $\eta = 2$ and $v_w = 340 \text{ km s}^{-1}$ for all galaxies; and
- (iv) **Momentum-conserving winds (vzw)**, where galaxies are identified on-the-fly and their velocity dispersion σ is estimated (see Oppenheimer & Davé 2008), and then

$$v_w = 3\sigma\sqrt{f_L - 1}, \quad (1)$$

$$\eta = \frac{\sigma_0}{\sigma}, \quad (2)$$

where $f_L = [1.05, 2]$ is the luminosity factor in units of the galactic Eddington luminosity (i.e. the critical luminosity necessary to expel gas from the galaxy potential), and $\sigma_0 = 150 \text{ km/s}$ is the normalization of the mass loading factor. Choices for the former are taken from observations (Rupke, Veilleux & Sanders 2005), while the latter is broadly is constrained to match high-redshift IGM enrichment (Oppenheimer & Davé 2008). The velocity dispersion σ is estimated from the baryonic galaxy mass M_{gal} using (Oppenheimer & Davé 2008)

$$\sigma = 200 \left(\frac{M_{\text{gal}}}{5 \times 10^{12} h^{-1} M_\odot} \frac{\Omega_m}{\Omega_b} \frac{H(z)}{H_0} \right)^{1/3} \text{ km/s}. \quad (3)$$

See Paper I for further details, and particularly note §2.2 for a discussion about issues related to the momentum budget in the vzw model.

2.2 Computing galaxy metallicities and gas fractions

We use SKID¹ (Spline Kernel Interpolative Denmax) to identify galaxies as bound groups of star-forming gas and

¹ <http://www-hpcc.astro.washington.edu/tools/skid.html>

stars (Kereš et al. 2005; Oppenheimer et al. 2010). Our galaxy stellar mass limit is set to be ≥ 64 star particles (Finlator et al. 2006), resulting in a minimum resolved mass of $M_{\text{gal}} = 1.1 \times 10^9 M_{\odot}$ in our r48n384 series of runs. We will only consider galaxies with stellar mass $M_* \geq M_{\text{gal}}$ in our analysis. We separate galaxies into central and satellite galaxies by associating each galaxy with a halo, where we identify halos via a spherical overdensity algorithm (Kereš et al. 2005).

To compute gas fractions, we set M_{gas} to be the mass of all star-forming gas in a SKID-identified galaxy. We then define

$$f_{\text{gas}} \equiv \frac{M_{\text{gas}}}{M_{\text{gas}} + M_*}, \quad (4)$$

where M_* is the stellar mass of the galaxy. Note that some authors choose $f_{\text{gas}} = M_{\text{gas}}/M_*$, and for instance, Peebles & Shankar (2010) argue that this definition is more natural in terms of understanding the origin of the MZR. Nevertheless, we prefer the above definition because it intuitively translates into the fraction of a galaxy’s (baryonic) mass that is in gas. In the end, so long as models and data are compared using the same quantity, the exact definition is not critical.

Our gas mass includes all phases of the ISM, including the cold neutral medium, molecular gas, and the warm ionized medium. The latter typically makes a small mass contribution, but the relation between the first two depends on the internal physics of the ISM (particularly self-shielding) that our simulations do not accurately track (see Popping et al. 2009, for further discussion). It is therefore important to compare to data that accounts for both neutral (H I) and molecular (H_2) components, as well as having been corrected for Helium. Furthermore, the determination of simulation gas content depends on the density threshold for star formation. Observationally, gas mass determinations can be sensitive to surface brightness effects in the outer regions of galaxies. Hence in general, gas fraction comparisons should be taken with some caution, and are mainly intended to illustrate trends.

The galaxy gas-phase metallicity is defined as the SF-weighted metallicity of all gas particles in SKID-identified galaxies. This definition most closely mimics how metallicities are measured observationally using nebular emission lines emanating from star-forming regions. We use the oxygen abundance as a metallicity tracer in our models, since this is also typical of observational determinations. We assume a solar oxygen mass fraction of 0.00574 (Asplund et al. 2009), or $[O/H]_{\odot} + 12 = 8.69$. The weighting of metallicity by star formation mitigates the issues regarding the outer regions of galaxies that plague gas fractions, since star formation is typically concentrated in the central region of the galaxy.

3 GALAXY METAL CONTENT

In this section we will examine the drivers behind the mass-metallicity relation (MZR) and its evolution out to high redshifts. We will focus on the physical mechanisms that connect inflows and outflows to the observable metal content of galaxies, in particular placing the form and evolution of

the MZR within the context of the equilibrium scenario for galaxy evolution.

3.1 The $z = 0$ mass-metallicity relation

Figure 1 shows the $z = 0$ relation between stellar mass and gas-phase metallicity, the MZR, in our simulations. The simulation data points are color-coded by star formation rate within bins of stellar mass, which we will discuss in §6. The main body of points comes from the r48n384 runs; the smaller-volume r24n256 run galaxies are shown as the sparser set of points at $M_* < 1.1 \times 10^9 M_{\odot}$ to extend the dynamic range. The magenta curve shows a running median, and the errorbars show 1σ deviations about the median. For comparison, the SDSS mass-metallicity relation mean (thick line) and 1σ scatter (dashed lines) is overlaid, but we will defer discussion of comparisons to observations until §5.

Metallicity measures have an uncertain normalization. This comes from uncertainties in metallicity determinations (e.g. Kewley & Ellison 2008), uncertainties in adopted metal yields (see discussion in Oppenheimer & Davé 2008), and uncertainties in the solar metal abundance (Asplund et al. 2009). Hence we treat the overall metallicity normalization as a free parameter. Given that we do not have any form of feedback that quenches massive galaxies in these runs (e.g. Gabor et al. 2011), our simulations most robustly model star-forming galaxies at masses below M^* . Therefore we normalize our metallicities to the observed MZR at $M_* \sim 10^{10} M_{\odot}$, where it so happens that all our wind simulations predict roughly similar metallicities. This normalization requires us to multiply all simulated metallicities by an arbitrary factor of 0.8. We apply this same factor at all redshifts and for all models. Hence the independent predictions of our simulations are the shape, slope, scatter, and evolution of the MZR, but not its overall amplitude.

All the wind models produce a general trend of increasing metallicity with mass and a turnover to flat at high masses. The no-wind case in contrast produces a nearly flat MZR, as one would expect from e.g. closed box evolution. All the wind models approach the no-wind case at $M_* \gtrsim 10^{11} M_{\odot}$, as these wind models all eject proportionally less material from the most massive galaxies, and the material that is ejected tends to quickly fall back in (Oppenheimer et al. 2010). If some form of ejective feedback to quench massive galaxies was included in our models (e.g. Gabor et al. 2011), this plateau metallicity may be lower.

While broadly similar, there are clear differences between various wind models. The constant wind model yields another turnover at low masses ($M_* \lesssim 10^{10} M_{\odot}$) towards a flat MZR. The slow wind model produces a similar turnover at somewhat smaller masses. The momentum-driven scalings case does not produce such a flattening, at least within the mass range probed by these simulations; the MZR slope here is nearly constant at $Z \propto M_*^{0.3}$ for $M_* \lesssim 10^{10.5} M_{\odot}$.

To understand the origin of these features for the various wind models, we review the findings from Finlator & Davé (2008) who developed a simple analytic understanding of the MZR. In their model, the gas-phase metallicity of a galaxy is set by a balance between inflow and outflow plus star formation. Inflow brings in low-metallicity

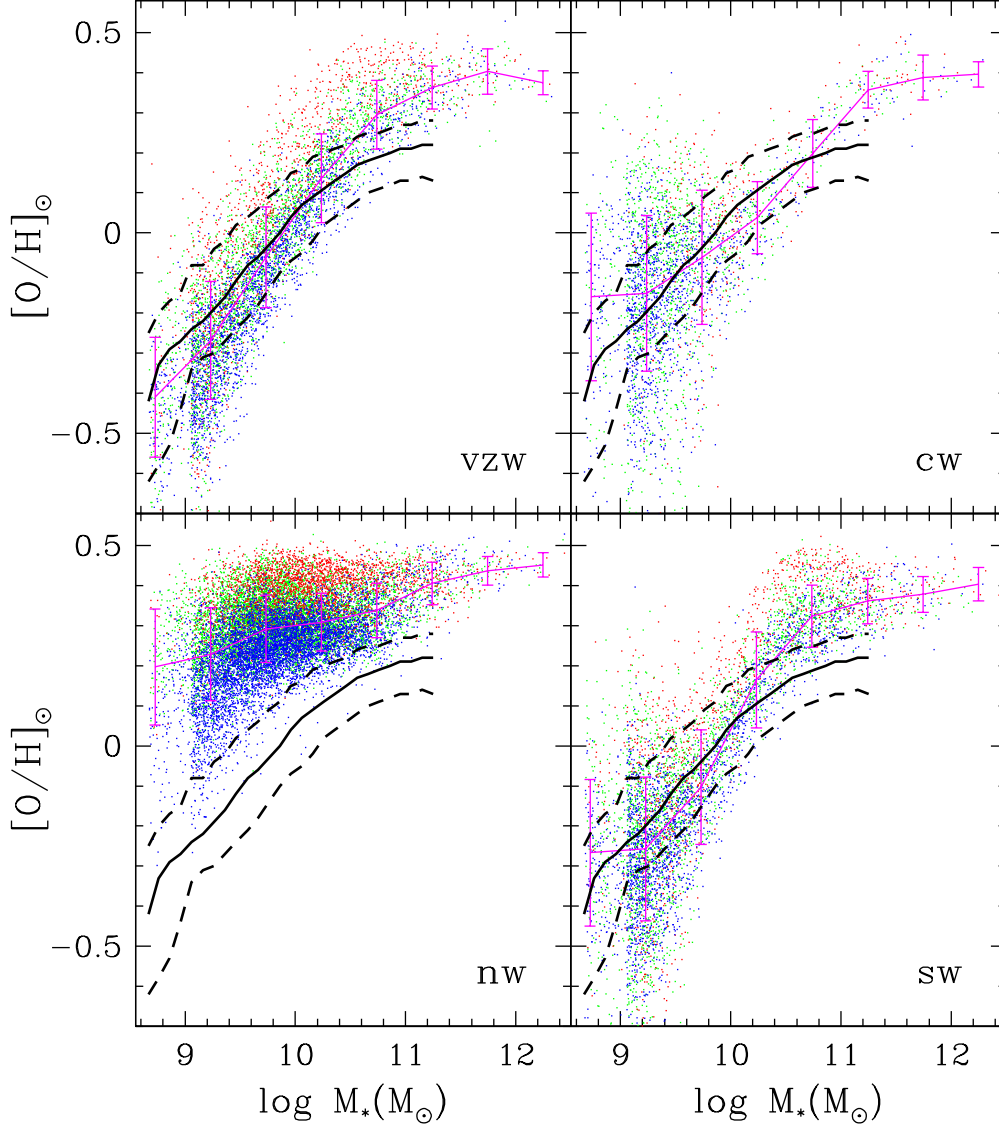


Figure 1. The M_* – Z_{gas} relation (MZR) at $z = 0$ in our r48n384 cosmological hydrodynamic simulations employing our four galactic outflow scalings: momentum-driven scalings (upper left), constant winds (upper right), no winds (lower left), and slow winds (lower right). Coloured points represent individual simulated galaxies, colour-coded by SFR within bins of M_* into upper (blue), middle (green), and lower (red) thirds. Magenta lines show a running median of the simulated points, with 1σ scatter about the median. The thick solid line is the $z \approx 0$ MZR from SDSS (Tremonti et al. 2004) with dashed lines showing the range enclosing 16% – 84% of the data. Note that all model oxygen abundances have been multiplied by 0.8 in order to match the amplitude of the observed MZR at $M_* \approx 10^{10} M_\odot$, which is within systematic uncertainties in metallicity measures; the shape, scatter, and evolution are independent predictions.

gas, star formation enriches that gas, while outflows modulate the fraction of inflow that turns into stars. In equilibrium, the three terms are related by

$$\dot{M}_{\text{inflow}} = \dot{M}_* + \dot{M}_{\text{outflow}}. \quad (5)$$

Rewriting this in terms of the mass loading factor $\eta \equiv \dot{M}_{\text{outflow}}/\dot{M}_*$, we obtain

$$\dot{M}_{\text{inflow}} = (1 + \eta)\dot{M}_* \quad (6)$$

In this simple “equilibrium” picture, the metallicity is given by the amount of metals produced by star formation, which is $y\dot{M}_*$ where y is the yield of metals per unit star formation, divided by the rate of gas inflow to be enriched. Hence

$$Z = y\dot{M}_*/\dot{M}_{\text{inflow}} = \frac{y}{1 + \eta}, \quad (7)$$

Here we have, for simplicity, assumed that the infalling gas has negligible metallicity; we will relax this assumption in §7 (see Equation 11).

It is worth noting that Equation 7 does not have any explicit dependence on stellar mass, but only depends on inflow and outflow rates. The physical interpretation is that the gas-phase metallicity does not reflect a historical record of star formation in a galaxy (as in a closed-box scenario), but rather reflects its recent (i.e. over a gas depletion timescale; §4.2) balance between inflows and outflows. This then distinguishes stellar metallicities, which must reflect the history of metal buildup, from gas-phase ones. In practice, however, the fairly slow evolution of the MZR (§3.2) means that galaxy stellar metallicities are only slightly lower than gas-

phase ones. We leave a detailed examination of stellar vs. gas-phase metallicities for future work.

Using Equation 7, we can understand the behavior of the various wind models. In the no-wind case, $\eta = 0$, and the metallicity is therefore close to constant. Although the MZR is close to flat, there remains a slightly slope owing to the rapidity of infall and the lack of reduction of fresh gas by outflows, which results in galaxies being not quite able to attain equilibrium. We will see in the next section that this effect becomes exacerbated at higher redshifts. Furthermore, there is more enriched infall into higher mass galaxies, as we discuss in §7.

The momentum-driven wind scalings assume $\eta \propto v_c^{-1} \propto M_*^{-1/3}$ (approximately). Hence when $\eta \gg 1$, this approximates $Z \propto M_*^{1/3}$. The turnover at high masses is set by the normalization of η , namely σ_0 , which produces $\eta \lesssim 1$ for $M_* \gtrsim 10^{11} M_\odot$ (at $z = 0$; this mass evolves mildly upwards with redshift). This interpretation differs from the canonical one (e.g. Tremonti et al. 2004) where the turnover is caused by the winds no longer being able to escape the potential well of the galaxy. In the momentum-driven scalings case, the wind speed scales with escape velocity, so even large galaxies eject material that can in principle escape (as observed e.g. for $z \sim 1$ galaxies by Weiner et al. 2009). However, the mass loading factors are low so they don't eject much material, and hence their metallicity is not suppressed.

The constant and slow wind cases introduce another consideration: The competition between wind speed and escape velocity. Unlike in the momentum-driven scalings where $v_w \sim v_{\text{esc}}$, here there is a transition mass above which the winds cannot escape, and fall quickly back into the galaxy. Hence the wind recycling time is very short, meaning that winds have little effect (Oppenheimer et al. 2010). This results in an *effective* mass loading factor that approaches zero above that threshold mass (see Finlator & Davé 2008 and §2.2 of Paper I). If one considers η in Equation 7 to be an effective mass loading factor, then at low masses $\eta = 2$ while at high masses $\eta = 0$ in these models, with a steep transition between these regimes across which the metallicity changes by a factor of $1 + \eta = 3$. Because the wind speed is twice as fast in the cw case, the transition occurs at a higher mass than in sw. Although the transition to the low-mass regime is not well probed at the dynamic range of these simulations (particularly in the sw case), it is still evident. This transition is also evident in the stellar mass and star formation rate functions in Paper I. This equilibrium scenario strongly predicts that the low-mass MZR will continue to be flat to small masses in this model.

These simulations and the associated equilibrium model indicate that the MZR is critically governed by the mass outflow rate from galaxies (i.e. η) and its scaling with M_* . This differs fundamentally from the canonical explanation for the MZR that invokes a competition between the galaxy potential well and the outflow velocity to modulate the metals retained within a galaxy (e.g. Dekel & Silk 1986; Dekel & Woo 2003; Tremonti et al. 2004); here, there is no mention of the potential well except via its effects on the mass loading factor. The way which η governs the MZR is by modulating the amount of mass that forms into stars, and thereby the amount of metals generated, from a given amount of inflow that is set by hierarchical structure growth. Hence the MZR is effectively governed by the “star formation efficiency”,

where here we mean this in the cosmological sense as the amount of infalling material that is converted into stars². This interpretation agrees with Brooks et al. (2007) who also found that the MZR is governed by the cosmological star formation efficiency, which is modulated by supernova feedback. In our models, this star formation efficiency is controlled by the rate at which mass is ejected in outflows.

3.2 MZR evolution

Figure 2 depicts the evolution of the MZR from $z = 3 \rightarrow 0$ in our four wind models. We show the running median at each redshift in the large panel, and the small panel below shows the 1σ variance about the median within each mass bin. The cyan points in the lower panels show the observed 1σ variance at $z \approx 0$ from SDSS data (Tremonti et al. 2004) for comparison; we will discuss this further in §6. We separately show the results for the r48n384 (solid lines), r24n256 (dotted), and r48n256 (dashed) runs; the good agreement at all overlapping masses indicates that these results are resolution-converged at least over the range of resolutions and volumes probed here. Although we don't show it here, all models at all epochs retain the second-parameter trend shown in Figure 1 wherein lower SFR galaxies at a given M_* have higher metallicities.

All the wind models have the general shape of their MZR as expected from the equilibrium model and described in the previous section. The shapes remain similar at all redshifts, because the form of $\eta(M_*)$ for each model does not change, and this governs the MZR shape as described in §3.1. The no-wind case appears further out of equilibrium at earlier epochs, as it deviates more strongly from the expected behavior of a constant metallicity at all masses. This is expected because accretion rates are higher at early epochs in comparison to gas processing rates within the ISM; we will discuss this further in §4.3. The trend of a metallicity increasing with time at a given M_* is quite generic, at least among the models considered here. This is not trivial; it is possible to design models that are quite reasonable in many ways but yield the opposite evolution (Arrigoni et al. 2010, and M. Arrigoni, priv. comm.).

In detail, the evolutionary rate at a given M_* varies somewhat with wind model. The momentum-driven wind scalings produce little early evolution, and more evolution from $z \sim 2 \rightarrow 0$. The constant- v_w models have less late evolution, particularly in the slow wind case, and more rapid evolution at early epochs. In Paper I we saw that such trends are also seen in the evolution of the galaxy star formation rate functions (Figure 2 of Paper I), where the constant- v_w cases evolved less out to $z \sim 2$ compared to the momentum-driven scalings case. This qualitative similarity in evolution is consistent with the interpretation that the MZR is governed primarily by galaxies' star formation rates, as suggested by Equation 7. We will discuss the evolution of the MZR further in §7, when we study how individual galaxies evolve in mass-metallicity space.

² This is notably different than the definition of star formation efficiency in the interstellar medium, which describes how quickly molecular gas is processed into stars.

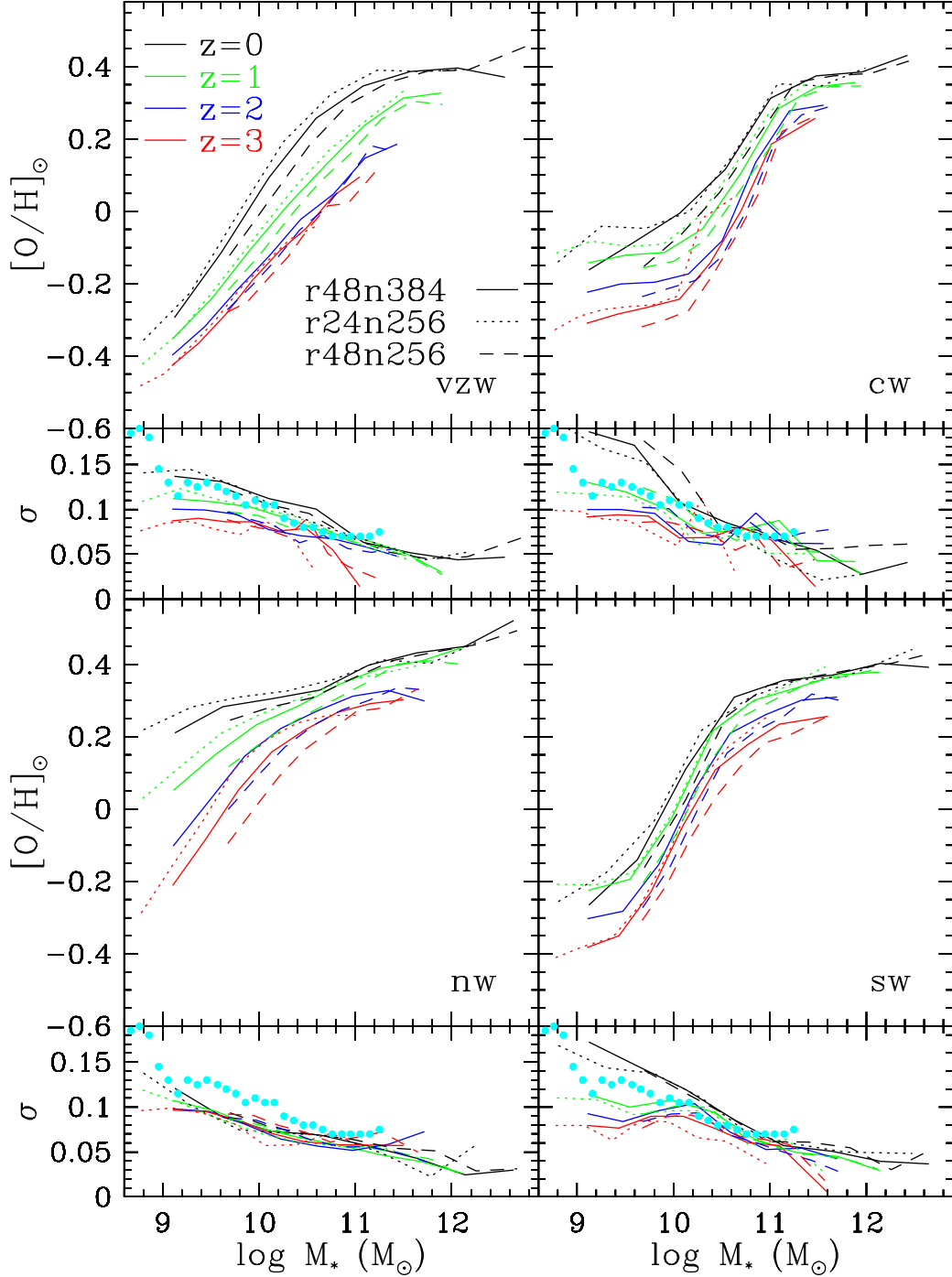


Figure 2. Large panels show the evolution of the mass-metallicity relation in our four wind models at $z = 0, 1, 2, 3$. Lines show the running median within mass bins at each redshift. Solid lines show the results from our r48n384 simulations, dotted lines show r24n256 runs, and dashed lines show r48n256 runs; the general consistency between the three indicates that the results are numerically converged, though the lowest resolution runs show noticeably lower metallicities. All models show an upwards evolution of metallicity at a given mass (at a rate that depends on wind model), although the characteristic MZR shape unique to each model does not change with redshift. Smaller panels below each large panel show the 1σ scatter about the median relation for all the models. Cyan points show the $\approx 1\sigma$ scatter in observations of the $z = 0$ MZR from Tremonti et al. (2004).

4 GALAXY GAS CONTENT

In this section we examine galaxy gas fractions and their evolution across cosmic time. As with the MZR, we attempt to provide physical intuition for what establishes a galaxy's

gas fraction and its evolution by connecting it to gas inflow and outflow processes.

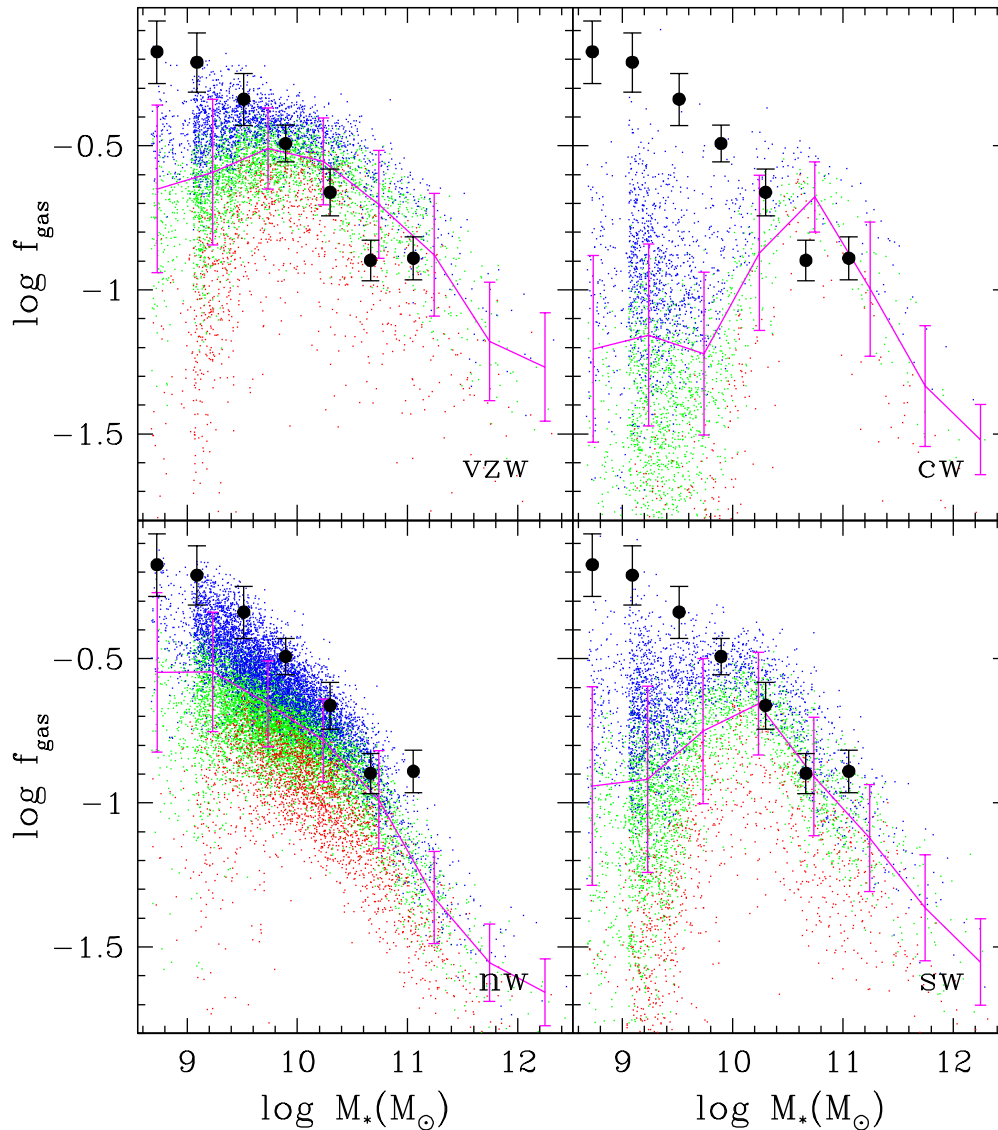


Figure 3. The relation between f_{gas} and M_* (MGR) at $z = 0$ in our four winds models, with magenta lines showing the median and 1σ scatter as in Figure 1. The points are color-coded by SFR within stellar mass bins: blue for upper third, green for middle third, red for bottom third. Data points show mean values as a function of M_* from a compilation of observations by Peeples & Shankar (2010).

4.1 Gas fractions at $z = 0$

Figure 3 shows the $z = 0$ gas fractions in our suite of simulations as a function of stellar mass (the mass-gas relation, or MGR). The points are color-coded by star formation within a given mass bin as in Figure 1; this will be discussed in §6. For comparison, the data points with errors show observed gas fractions ($\text{H I} + \text{H}_2$), corrected for Helium, compiled and binned by Peeples & Shankar (2010).

At the massive end, all models show decreasing gas fractions with stellar mass. At lower masses, however, all wind models eventually deviate from this trend, displaying a maximum typical gas fraction below which the gas fraction becomes lower to smaller masses. The no-wind case shows no such maximum. The mass at which this maximum occurs appears to be related to wind recycling, i.e. the return of previously-ejected material back into a galaxy. Oppenheimer et al. (2010) showed that the recycling time

becomes long at smaller masses, eventually exceeding a Hubble time. The mass at which the recycling time becomes longer than the Hubble time in each wind model is, to a good approximation, the mass at which the maximum gas fraction is seen. This suggests that the lower gas fractions at small masses occurs at least in part because ejected winds never return to these galaxies.

As emphasized by van de Voort et al. (2010) and Faucher-Giguere, Kereš, & Ma (2011), feedback adds energy to surrounding gas and prevents material from entering into smaller galaxies. Since much of the material entering into galaxies' ISM at $z = 0$ is recycled winds (Oppenheimer et al. 2010), the majority of the effect is that small galaxies do not re-accrete their winds. The constant wind model shows the highest turnover mass in f_{gas} , while the slow wind and momentum-driven scalings cases occur at lower masses. The latter wind model also shows a somewhat slower drop-off in

f_{gas} to lower masses, reflecting its less steep dependence of recycling time with mass.

Another possible issue is that perhaps many low-mass galaxies are satellites that have lower gas content owing to stripping or strangulation processes. However, we will show in §6.3 that the satellite fraction does not increase appreciably to small masses, and we will demonstrate that the turn-down in gas fractions to small masses is present in both satellites and centrals. Hence this particular trend does not arise from satellites, although other interesting trends do that we will explore in §6.3.

The non-monotonic behavior of gas fractions in wind models reflects a similar behavior, with similar characteristic scales, as the specific star formation rate ($\text{sSFR} \equiv \text{SFR}/M_*$) examined in Paper I. There we saw that low-mass galaxies had depressed sSFRs relative to an extrapolation from higher masses in all wind models; the no-wind case showed no such deviation. This trend arises because of a combination of wind recycling, which brings extra accretion at high masses (Oppenheimer et al. 2010), and preventive feedback which suppresses accretion into galaxies at the lowest masses (e.g. van de Voort et al. 2010). The suppression of gas fractions is seen to be directly proportional to the suppression in sSFRs, which we will explain in §4.3. Hence the discrepancies of models relative to observed sSFRs of dwarf galaxies noted in Paper I is directly traceable to lowered gas fractions in dwarfs predicted in models.

In summary, gas fractions fall with mass at the highest masses but show a turnover at low masses in all the wind models. This turnover is not seen in observations, as we will discuss in §5. To understand the origins of these trends, and also gas fraction evolution, let us examine an instructive quantity for understanding gas processing in galaxies, namely the depletion time.

4.2 Depletion time

Figure 4 shows the gas depletion time t_{dep} as a function of stellar mass in our four wind models, from $z = 3 \rightarrow 0$. We define $t_{\text{dep}} \equiv M_{\text{gas}}/\text{SFR}$, which is the time that galaxy would take to consume its current gas supply at its current star formation rate. Our three sets of simulations for each wind model are shown to demonstrate good resolution convergence over the dynamic range probed. To illustrate a useful trend, we divide t_{dep} by the Hubble time t_H at each redshift.

Several general features of $t_{\text{dep}}(M_*, z)$ are evident in Figure 4: First, higher-mass galaxies have shorter depletion times. Second, depletion times are, to first order, independent of wind model. Finally, t_{dep}/t_H is essentially invariant over most of cosmic time. The insensitivity to wind model and invariance when scaled to the Hubble time provide key clues into the physics governing t_{dep} , and in turn, galaxy gas contents.

We can broadly understand these trends using a straightforward argument based on our star formation law. The depletion time measures how gas, once within a galaxy, gets consumed into stars. Our simulations model conversion of gas to stars by assuming a Kennicutt-Schmidt Law, which equivalently follows the relation that the star formation rate is the gas mass divided by the dynamical time t_{dyn} (of the star-forming disk), times some overall efficiency fac-

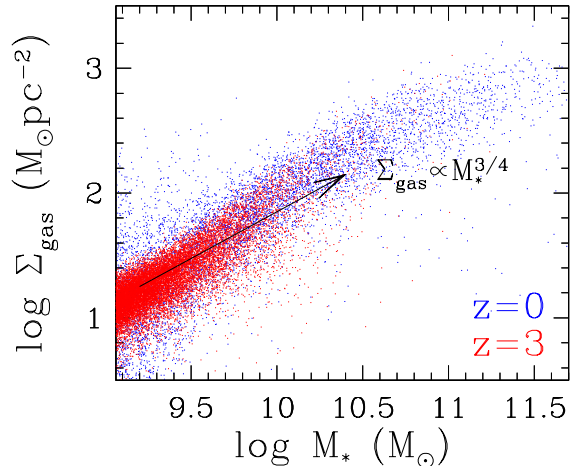


Figure 5. Gas surface density Σ_{gas} versus stellar mass M_* in galaxies from our r48n384vzw simulation, at $z = 0$ (blue) and $z = 3$ (red). The gas surface density is taken to be the gas mass divided by πR^2 , where R is the stellar half-mass radius of the galaxy. This relation is reasonably well described by $\Sigma_{\text{gas}} \propto M_*^{3/4}$, as shown by the arrow.

tor that is measured to be around 2% both locally and in distant galaxies (e.g. Genzel et al. 2010). Hence the depletion time should scale as the dynamical time. In a canonical disk model (Mo, Mao, & White 1998), the dynamical time evolves as t_H , and hence we expect t_{dep}/t_H to be approximately constant, which is generally confirmed in Figure 4, although with deviations at low masses at $z = 0$ that we discuss below.

The mass dependence of t_{dep} depends on the conversion rate of gas into stars. This is set by the details of internal structure of galaxies within our simulation along with the assumed Kennicutt-Schmidt star formation law, which is $\Sigma_{\text{SF}} \propto \Sigma_{\text{gas}}^{1.4}$ where Σ_{SF} and Σ_{gas} are the surface densities of star formation and star-forming gas, respectively. Hence $t_{\text{dep}} = \Sigma_{\text{gas}}/\Sigma_{\text{SF}} \propto \Sigma_{\text{gas}}^{-0.4}$.

We then employ an empirical relation measured in our simulations of $\Sigma_{\text{gas}} \propto M_*^{3/4}$ that we show in Figure 5. It does not evolve appreciably with redshift. While we do not explicitly show it, this relation holds reasonably well for all the wind models. Observations of the stellar mass density profile in late-type SDSS galaxies indicate $\Sigma_* \propto M_*^{0.54}$ (Kauffmann et al. 2003), which is slightly shallower. Gas profiles are more difficult to measure, but at least in our models, star-forming gas generally traces stars. Using this shallower slope would not significantly change our results, but we prefer to use the simulated slope since we are trying to develop an analytic understanding of the simulation results. Our r24n256 and r48n256 simulations have slightly different amplitudes for this relation but the slope is identical, suggesting that the trend with M_* is insensitive to resolution at least over the (admittedly narrow) range probed by these simulations.

Putting this together, we obtain

$$t_{\text{dep}} \propto t_H M_*^{-0.3}. \quad (8)$$

This scaling provides a good match to $t_{\text{dep}}(M_*)$ in our sim-

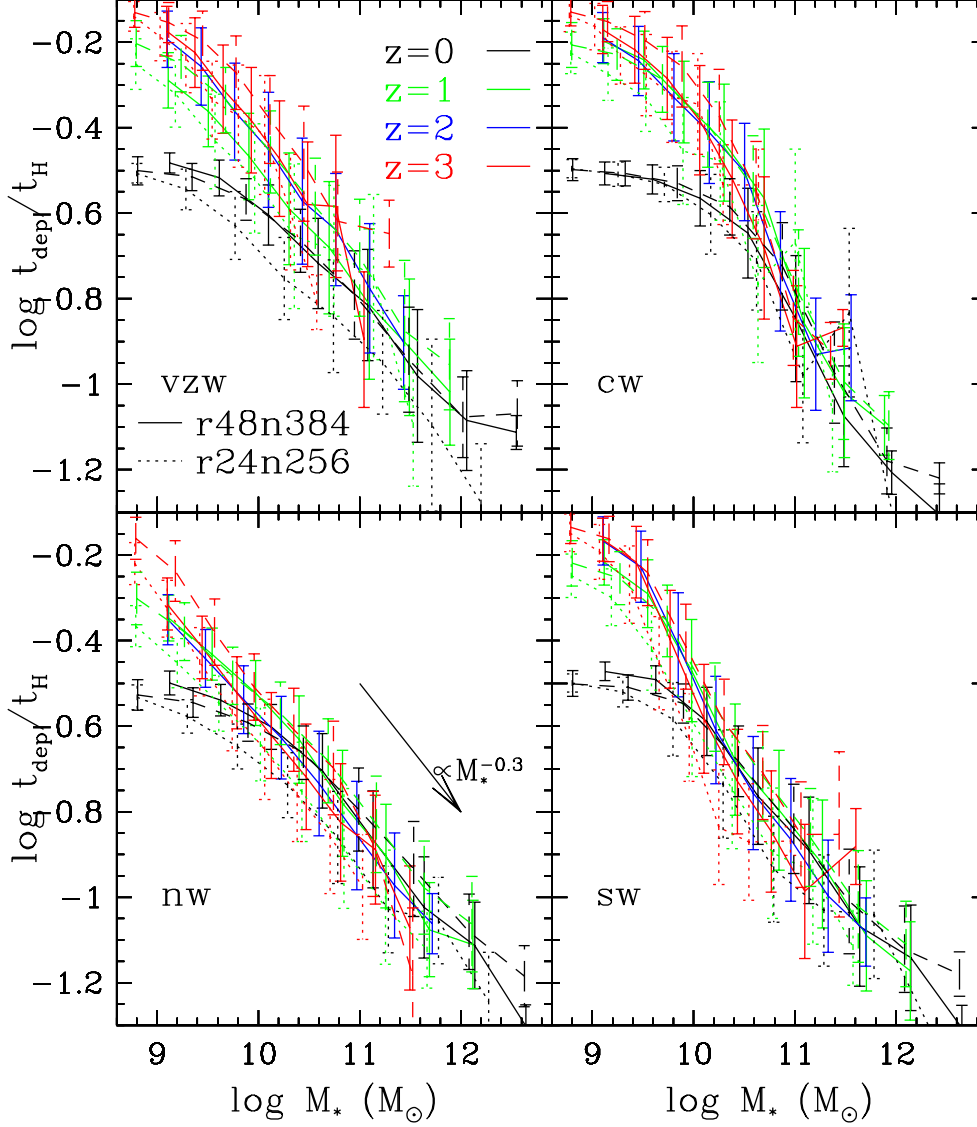


Figure 4. Depletion time $t_{\text{dep}} \equiv M_{\text{gas}}/\text{SFR}$ in units of the Hubble time t_H in our four wind models at $z = 0, 1, 2, 3$. Solid lines show results for the r48n384 series, dotted lines show r24n256, and dashed lines show r48n256. t_{dep} drops to larger masses roughly as $M_*^{-0.3}$ and scales with t_H , essentially independent of winds, as derived in Equation 8.

ulations at most epochs and masses as shown in Figure 4. Since we assume the same star formation law in all our wind models, there is little sensitivity to outflows in this relation.

We note that $t_{\text{dep}} \propto t_H$ does not necessarily have to be the case – for instance, in mergers, t_{dyn} is quite small within the dense central star-forming region during the starburst phase, meaning that t_{dep} of such starburst galaxies should lie below the mean relation. The relatively tight relation of $t_{\text{dep}}(M_*)$ in our models indicates that, in analogy with the tight main sequence (Davé 2008, Paper I), mergers are not a dominant population at any redshift. Hence even though we

have not explicitly used the equilibrium condition in deriving t_{dep} , the connection between global virialization and the properties of the star-forming region in galaxies only holds when galaxies are in a steady-state situation.

t_{dep} is to first order insensitive to outflows; all models, regardless of winds, show a roughly similar $t_{\text{dep}}(M_*)$. This is expected since the derivation of Equation 8 does not involve any aspect that depends on outflows, effectively employing only the star formation law and virial arguments. This supports the idea of Paper I that star formation is supply-regulated, that is, star formation oc-

curs in proportion to the gas available to form stars. This differs relative to expectations from models in which galaxies begin with a large reservoir of gas and consume them rapidly (e.g. Eggen, Lynden-Bell, & Sandage 1962; Maraston et al. 2010).

At $z = 0$, we see a systematic departure from the mean trend towards lower t_{dep} at low masses. Part of this owes to satellite galaxies that are increasingly starved of gas to low masses at low redshifts (Figure 6 of Paper I), which occurs even in the no-wind case. In the wind models, an additional role is played by preventive feedback and the lack of wind recycling at small M_* . As usual for effects involving wind recycling, the departure from the canonical relation occurs at a higher mass in cw relative to sw, and is more gradual in the vzw case. These effects are very mild at earlier epochs when wind recycling is not as common.

The depletion time has sometimes been interpreted as a measure of star formation efficiency variation with galaxy mass, such that more massive galaxies more efficiently convert gas into stars. But in our models, the star formation efficiency is an input constant that is calibrated to match observations of present-day disks (Springel & Hernquist 2003b; Oppenheimer & Davé 2008), and does not vary with galaxy mass. The trend of t_{dep} with M_* arises from the assumed star formation formation law, which is why it is very weakly dependent on details of feedback.

4.3 Gas fraction evolution

Figure 6 shows the evolution of the MGR from $z = 3 \rightarrow 0$ in our simulation suite. Following Figure 2, the solid lines show medians with 1σ spread for the r48n384 runs, while the dotted and dashed lines show likewise for the r24n256 and r48n256 runs, respectively. Once again, good resolution convergence is seen, as all the key features are reproduced at each resolution, although we emphasize that the dynamic range probed here is only a factor of eight in mass. The smaller panels show the running 1σ variance about the median, and cyan points show the observed scatter from Peebles & Shankar (2010).

All models display a slowly falling gas fraction with time at a given mass, while the variances (small lower panels) become slightly higher with time. Hence higher- z galaxies are more gas-rich, in qualitative agreement with observations. The fundamental physics governing this is a competition between gas inflow and gas consumption rates. In the cold accretion paradigm, the amount of gas inflowing into the star forming region is proportional to the gas inflowing at the halo virial radius, since cold streams channel material to the center of the halo (Dekel et al. 2009). In detail, preventive feedback mechanisms can reduce ISM inflow (van de Voort et al. 2010; Faucher-Giguere, Kereš, & Ma 2011) particularly at low masses.

The amount of gas entering the virial radius can be estimated by the total mass accretion rate times the baryon fraction, which scales as $(1+z)^{2.25}$ (Dekel et al. 2009). Meanwhile, the gas consumption rate is given by how fast gas can be processed into stars or an outflow, which is given by $t_{\text{dep}}/(1+\eta)$. Since $t_{\text{dep}} \propto t_H$, at any given mass (which approximately corresponds to a given η), the consumption rate is given by t_H^{-1} . Since t_H^{-1} evolves with z slower than

$(1+z)^{2.25}$ (e.g. $t_H^{-1} \propto (1+z)^{1.5}$ in the matter-dominated era), it is straightforward to see that the gas supply rate drops faster with time than the gas consumption rate. This explains why galaxies start out gas-rich but then the gas fraction drops as the gas consumption rate catches up.

While the naive notion that galaxies simply “consume their gas” is qualitatively in accord with observations, the rapid consumption times (Tacconi et al. 2010) imply that gas must be continually supplied. In our simulations, this indeed happens, but at a rate that becomes slower with time (relative to the consumption rate), causing a gas fraction that slowly drops. The no-wind case in Figure 6 shows a self-similar (in M_*) downwards evolution in f_{gas} arising from this scenario.

We can quantify these scalings and gain more insight into gas fractions by first using the definition of t_{dep} to rewrite

$$f_{\text{gas}} = \frac{1}{1 + t_{\text{SF}}/t_{\text{dep}}}, \quad (9)$$

where $t_{\text{SF}} \equiv M_*/\text{SFR} = 1/\text{sSFR}$. Thus the dependence of f_{gas} on mass and redshift reflects the dependence of the ratio $t_{\text{SF}}/t_{\text{dep}}$ on these quantities.

Let us consider the redshift evolution first. In Paper I we showed that the observed t_{SF} at $M_* = 10^{10} M_\odot$ was consistent with following the trend predicted by halo accretion, namely $t_{\text{SF}} \propto (1+z)^{-2.25}$, from $z \sim 2 \rightarrow 0$. Figure 4 shows that $t_{\text{dep}} \propto t_H$ over that time, albeit with some deviations at low- z at low masses. Hence the ratio $t_{\text{SF}}/t_{\text{dep}}$ rises with time, approximately as $(1+z)^{0.75}$ at high- z and $(1+z)$ at low- z , resulting in a dropping gas fraction. Since t_{SF} and t_{dep} are to rough order independent of winds, this explains the basic behavior of f_{gas} dropping with time in all models.

Equation 9 can also be used to gain insights on the mass dependence of f_{gas} . At larger masses (e.g. $M_* \gtrsim 10^{10} M_\odot$), $t_{\text{dep}} \ll t_{\text{SF}}$, so we can approximate $f_{\text{gas}} \approx t_{\text{dep}} \text{sSFR}$. Consider first the no-wind case, here $\text{sSFR} \propto M_*^{-0.2}$ (approximately; see Figure 2 of Paper I). Combined with $t_{\text{dep}} \propto M_*^{-0.3}$ (Equation 8), this then roughly predicts $f_{\text{gas}} \propto M_*^{-0.5}$. This slope is indicated in the nw panel of Figure 6, and provides a good fit to the high-mass slope of $f_{\text{gas}}(M_*)$. At lower masses, once $t_{\text{dep}}/t_{\text{SF}}$ becomes a significant fraction of unity, the gas fraction levels off.

In the wind models, f_{gas} will reflect features seen in the sSFR, and at $z = 0$ there are additional deviations owing to t_{dep} . In general, sSFRs in the wind models show a turnover to lower sSFRs at low masses (Figure 3 of Paper I). The location and strength of that turnover depends on the particular wind model, owing to wind recycling as discussed in Paper I. At high masses, sSFR in wind models is raised over the no-wind case by wind recycling, which is more rapid in higher mass galaxies. At low masses, the sSFR is lowered owing to preventive effects of winds adding energy to surrounding gas (e.g. Oppenheimer et al. 2010; van de Voort et al. 2010). These trends are directly reflected in $f_{\text{gas}}(M_*)$: At high masses, they are somewhat larger than the no-wind case, while they all show a turnover to low gas fractions at low masses. At $z = 0$, this reduction at low masses is exacerbated by the drop in t_{dep} to low masses.

An interesting regime that is not probed here is the very high- z epoch ($z \gtrsim 3$). At sufficiently high redshifts, the rapidly-rising accretion rate will begin to exceed the less

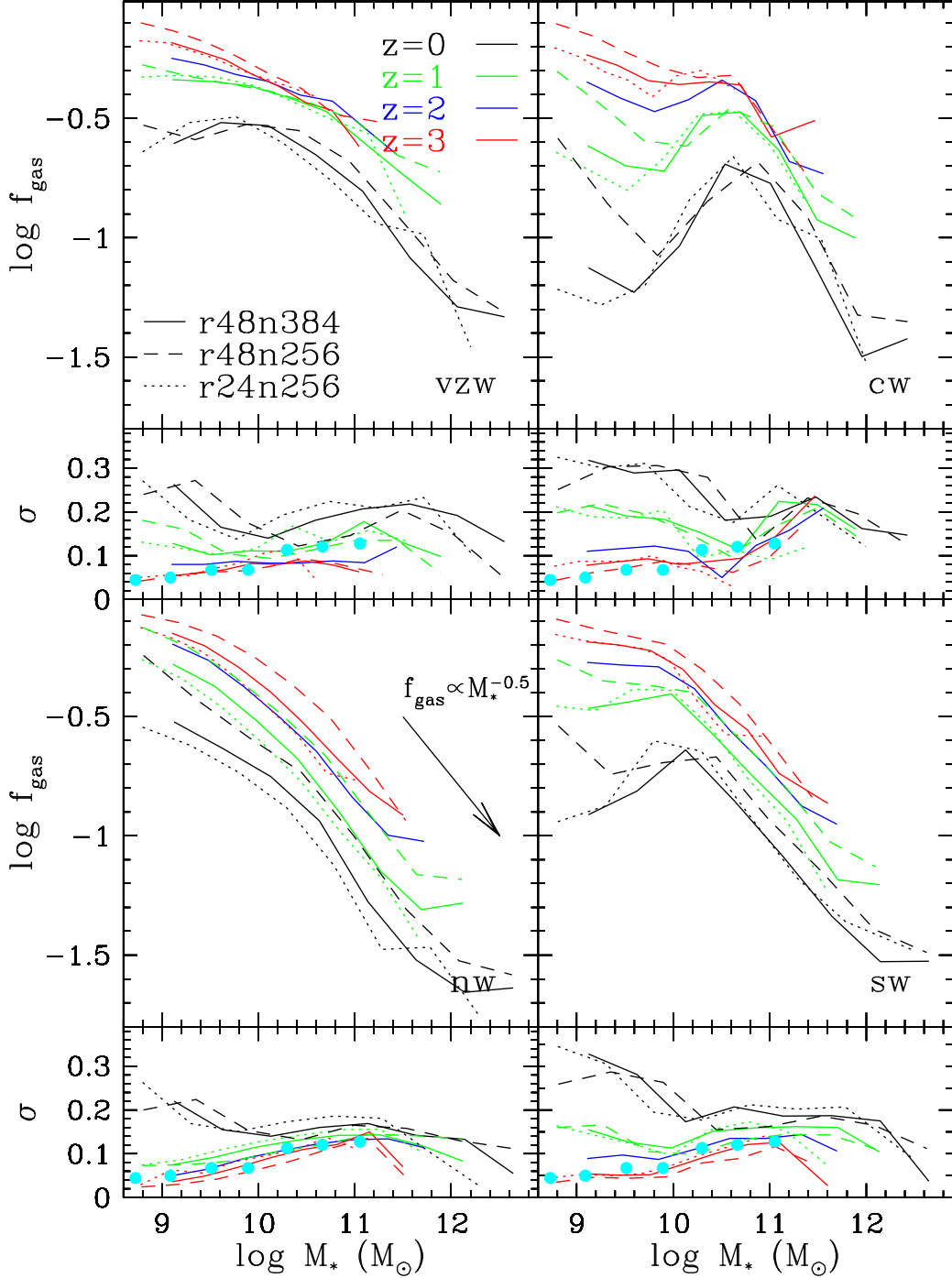


Figure 6. Like Figure 2, only for gas fraction, showing the evolution of the MGR in our four wind models at $z = 0, 1, 2, 3$. Cyan points show the observed scatter from Peebles & Shankar (2010). The arrow in the no-wind panel shows a slope of -0.5 , as is roughly expected at the high-mass end; see text.

rapidly-rising gas consumption rate. In that case, star formation cannot keep up with the gas supply, and the galaxies will no longer be in equilibrium. This is then the *gas accumulation phase*. The exact epoch where this happens depends on feedback; when outflows are highly mass loaded, the amount of infalling gas that needs to be processed into stars is reduced, and equilibrium can occur earlier on. Also, there is some mass dependence because t_{dep} has a significant mass dependence (Figure 4), but t_{SF} (or sSFR) is essentially

independent of mass at high- z (González et al. 2010). Interestingly, there are now empirical constraints on the gas accumulation epoch: Papovich et al. (2010) showed, based on modeling the evolution of the luminosity and sizes of high-redshift Lyman break galaxies, that at $z \gtrsim 4$ the global gas accretion rate exceeds the star formation rate, while below that redshift they track each other.

In summary, the evolution of gas fractions reflects a competition between cosmic inflow and gas consumption

rates. A quick estimate of their scalings shows that cosmic inflow abates faster than gas consumption, resulting in dropping gas fractions with time in all models. Outflows provide higher-order modifications to this picture, particularly owing to wind recycling and preventive feedback effects at late times. These trends can be understood by considering the dependence of the specific SFR (i.e. t_{SF}) and the depletion time t_{dep} on mass and redshift. At sufficiently early epochs, inflow will be so rapid that gas processing cannot keep up, resulting in a gas accumulation phase.

5 COMPARISONS TO DATA

While the main purpose of this paper is to understand how galactic inflows and outflows impact the gas and metal content of galaxies, it is instructive to see how our suite of models compares to key observations of these quantities out to high redshifts. We have already seen that different outflow models generate significantly different predictions for gas and metal content. Here we compare to a recent sample of forefront observations to see how they constrain our outflow models.

Figure 7 shows a comparison of the mass-metallicity relation (top panels) and the mass-gas fraction relation (bottom panels) to observations (in black and cyan) at $z = 0, 2, 3$. The $z = 0$ metallicity observations are taken from Tremonti et al. (2004), and the gas fraction data from a compilation by Peeples & Shankar (2010). At $z = 2$, we show metallicities and gas fractions from Erb et al. (2006); the gas fractions here are inferred from the star formation rate surface density and assuming the Kennicutt-Schmidt Law. We also show (in cyan) “direct” gas fraction measures from Tacconi et al. (2010) using CO measurements plus an assumed conversion of CO to H_2 . At $z = 3$, we compare to data from Mannucci et al. (2010), which is from a sample of Lyman break galaxies at $z \sim 3 - 4$ (black points), and from Richard et al. (2011) from a sample of lensed galaxies at $z = 2.5 - 3.1$ (cyan points, metallicities only).

Looking at the $z = 0$ MZR, the only model that is clearly discrepant is the one with no winds. Galaxies are (not surprisingly) over-enriched, because this model greatly overproduces the stellar content of galaxies (see e.g. Paper I). Other works have argued that the $z = 0$ MZR can be reproduced by varying the ISM star formation efficiency, i.e. the rate of gas consumption in the ISM, or the IMF (Köppen, Weidner, & Kroupa 2007). In our simulations, the IMF is always assumed to follow that of Chabrier (2003), and the gas depletion timescale t_{dep} is essentially the same in all our models including no-wind. Hence in our models, these factors are not responsible for the differences in the MZR. In our equilibrium model (eq. 7), the no-wind model overproduces metals because it does not eject ISM material to suppress star formation. This in some sense represents a “cosmological” star formation efficiency, i.e. the amount of cosmic infall that is converted into stars. In our models (like those of Brooks et al. 2007), the MZR is governed by the cosmological star formation efficiency rather than the ISM one.

The wind models are generally all in the ballpark of the $z = 0$ SDSS data, but they show non-trivial discrepancies. At the massive end, all models overproduce the metal-

licities in $M_* > M^*$ galaxies. Recall that we have arbitrarily scaled all our metallicities to match observations at $M_* \sim 10^{10} M_\odot$, so we cannot improve overall agreement by rescaling our yields or metallicity indicators further. One possible reason is that there is another feedback mechanism that kicks in at $M_* \gtrsim M^*$. As we saw in Paper I, this is already required for suppressing star formation in massive systems (e.g. Gabor et al. 2011); it would not be surprising if it also suppressed metallicities. We note that the observed SDSS sample is solely emission-line galaxies, so does not include “red and dead” systems; nevertheless, as shown in e.g. Salim et al. (2007) and Paper I, even star-forming systems seem to have suppressed star formation at the massive end compared with a simple extrapolation from lower-mass systems. Another possibility is that wind recycling is bringing in highly enriched material that is elevating the galaxy metallicities. Hence this discrepancy may suggest that the impact of wind recycling is overestimated in these simulations. In any case, quantitatively matching both the mass function and the MZR plateau may provide interesting constraints on such feedback mechanisms.

At the low-mass end, all wind models remain within the observed 1σ variance among SDSS galaxies down to the lowest masses probed here ($M_* \sim 10^9 M_\odot$). However, the equilibrium model predicts that the simulations with constant η should have a flat MZR at low masses (eq. 7). This flattening trend is clearly visible in the cw run, and less so in the sw case since it kicks in at lower masses. Unfortunately we do not yet have the computing power to resolve smaller systems within a representative $z = 0$ cosmological volume to confirm this prediction directly, but higher-resolution runs done to $z = 2$ do show this trend (Finlator & Davé 2008). Observationally, Lee et al. (2006) has found that the MZR continues with a similar slope down to $M_* \sim 10^6 M_\odot$. This would clearly be discrepant with expectations for the constant- η cases, and would favor models where there is progressively higher η at lower masses as in momentum-driven wind scalings.

The mass-dependent MZR evolutionary rates among wind models offer an opportunity to constrain such models by comparisons with higher- z data. The no wind model continues to over-enrich galaxies by $\sim \times 2 - 3$, but the slope is now in better agreement. It would be surprising if uncertainties in yields, metallicity measures, etc. could conspire to produce a $\times 2 - 3$ change in metallicities, but we cannot rule out that possibility. But we disfavor this idea because the no-wind model also grossly overproduces the amount of stellar mass at $z = 2$ (as at all redshifts; see e.g. Paper I), so it would be highly surprising if it produced the proper metal content in galaxies.

In terms of wind models, at $z = 0$ the sw model was a reasonable fit, but at $z = 2$ it substantially over-enriches galaxies. Since there are few red and dead galaxies at this epoch, over-enrichment at the massive end is likely to be a serious defect that will not be alleviated by quenching (e.g. AGN) feedback. The cw model also produces the wrong shape for the MZR, as discussed in Finlator & Davé (2008). Recall that the MZR shape is probably the most robust predictions of our simulations, so again this is a serious defect. Meanwhile, the momentum-driven scalings case is a reasonable match in terms of shape and amplitude (modulo that

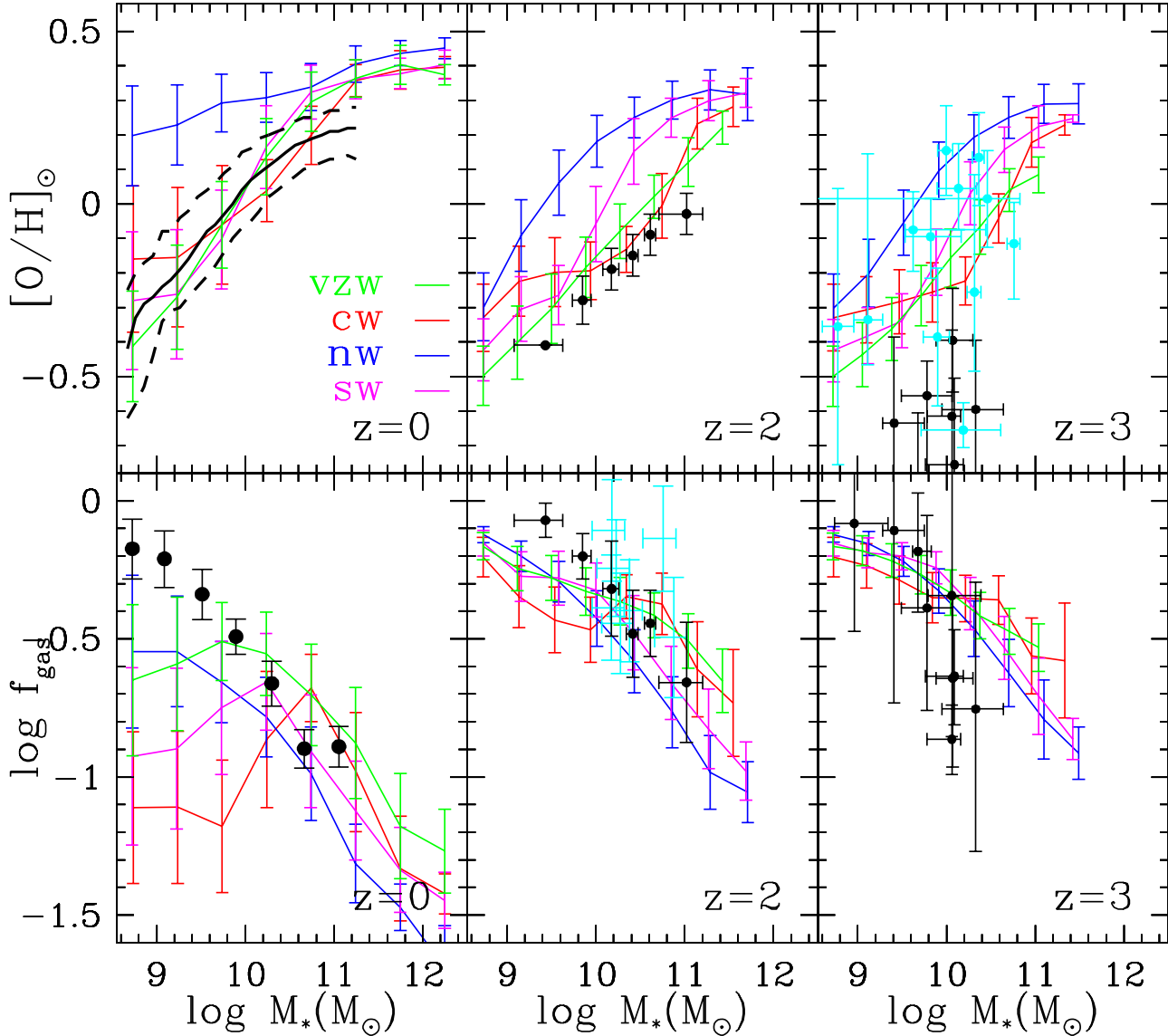


Figure 7. A comparison to observations for the mass-metallicity (top panels) and mass-gas fraction (bottom panels) relation in our four wind models at $z = 0, 2, 3$ (left to right panels). Lines with error bars show the running median and 1σ variance within mass bins from our r48n384 runs. Data points show the MZR at $z = 0$ from SDSS (Tremonti et al. 2004, solid line with 16% – 84% enclosing errorbars), at $z = 2$ from Erb et al. (2006) and at $z = 3$ from Mannucci et al. (2010, $z \sim 3 - 4$; black points) and Richard et al. (2011, $z \sim 2.5 - 3.1$; cyan points). The momentum-driven wind scalings case comes closest to matching at both $z = 0$ and $z = 2$ of the models here. For gas fractions, $z = 0$ data is shown from a compilation by Peebles & Shankar (2010), at $z = 2$, indirect gas fractions from Erb et al. (2006b, black points) and direct (CO-based) gas fractions from Tacconi et al. (2010, cyan), and at $z = 3$ from Mannucci et al. (2010). The momentum-driven wind scalings provide the overall best match, but are still discrepant at $M_* \lesssim 10^{9.5} M_\odot$; note that current samples measuring gas fractions generally do not include gas-poor galaxies that are often (in our models) satellites.

we have scaled all our metallicities in all wind models by a factor of 0.8).

At $z = 3$, the metallicity data from Mannucci et al. (2010) lies well below all model predictions, while the data from Richard et al. (2011) is in good agreement. Since the former sample averages a slightly higher redshift, this might imply very rapid evolution in the MZR during the short time from $z \sim 3.5 \rightarrow 2.5$, but this is very difficult to reconcile with the observed (and predicted) slow evolution from $z \sim 2.5 \rightarrow 0$. Models can usually match data at two of the

three epochs, but no model that we are aware of can match all three epochs when considering the Mannucci et al. (2010) data. One possibility is that there are observational selection effects coming into play, because the Mannucci et al. (2010) $z > 3$ sample consists of rest-ultraviolet (UV) selected galaxies, while the Richard et al. (2011) sample consists of lensed galaxies. Rest-UV selection will tend to pick out high-SFR systems, which in turn have low metallicities for their M_* (see Figure 1, with a more detailed discussion in §6). It remains to be seen if selection effects can quan-

titatively reconcile the models and data. Another possibility is that there are differences in the poorly-understood calibrations of metallicity indicators (e.g. Kewley & Ellison 2008), although both works claim to have carefully considered this. Investigating the origin of the differences in the observations is beyond the scope of this work, so we merely take these as reflective of current systematic uncertainties in high- z MZR measures. Upcoming surveys such as the Spitzer Extragalactic Deep Survey (SEDS) and the Cosmic Assembly Near-infrared Deep Extragalactic Legacy Survey (CANDELS) will yield many stellar mass-selected galaxies at these redshifts, offering opportunities through follow-up spectroscopy to measure metallicities in large homogeneous samples.

Turning to gas fractions, at $z = 0$ all models produce the observed trend of lower gas fractions in more massive systems. As discussed in §4.3, the trend in massive (i.e. low- f_{gas}) galaxies is set by the depletion time times the specific SFR; these both drop with mass, albeit mildly. The gas fractions in the no-wind case follow the observed shape but are too low. One might try to reconcile this by noting that the model definition of gas fraction as all star-forming gas (i.e. gas above $n = 0.13 \text{ cm}^{-3}$) may not be directly comparable to observational measures of f_{gas} . But at least at face value, the no-wind model appears to consume too much of its gas into stars by $z = 0$, leaving galaxies too gas-poor and consistent with its overproduction of stars and metals.

At $z = 0$, the wind models are broadly in the range of observations at high masses, but in all cases they show a turnover in gas fractions at low masses that is clearly in disagreement with observations. Hence something in the current wind simulations is either removing too much gas from dwarfs, not supplying enough gas to them, and/or consuming their gas too quickly. In Paper I we suggested that one explanation may be that the star formation law is different in these systems (as argued by e.g. Robertson & Kravtsov 2008), particularly at low- z when they are typically fairly low surface brightness objects, or that the conversion of neutral into molecular hydrogen is less efficient (Krumholz, Leroy, & McKee 2011). It is curious that the simulation without winds at least generally shows the correct trend to the lowest masses, and hence another possibility is that preventive feedback effects owing to winds are incorrectly modeled in these outflow simulations.

There are other possibilities for the low-mass f_{gas} discrepancy. For instance, there are more quenched satellites at low masses (Figure 4 of Paper I) which have been depleted of gas. However, as we will show in §6.3, even central dwarf galaxies show a turnover in f_{gas} . Finally, there may be observational selection effects in the data as gas mass observations (particularly of small systems) tend to focus on gas-selected (e.g. H I) galaxies. For instance, to reconcile the vzw model at the lowest mass bin ($M_* \sim 10^9 M_\odot$) requires that observed galaxies are typically 2σ outliers in gas fractions, which is not impossible. Upcoming surveys such as the Galex Arecibo SDSS Survey (GASS; Catinella et al. 2010) that measure the gas content in an unbiased sample will be helpful, but are not targetted to the lowest mass systems where the largest discrepancies arise. The gas content of low-mass galaxies is therefore an important barometer for models, and further data and modeling are needed to shed light on whether this is indeed a serious discrepancy.

At higher redshifts, gas fraction measurements become quite uncertain. At $z \sim 2$, all models are in fair agreement with observations, although the data overall tend to show somewhat higher gas fractions. Selection effects again may play a role, since these galaxies tend to be selected as having either high gas content (so that direct measures are feasible) or high star formation rate (which implies high gas content; Figure 3). Indirect gas fractions as used by Erb et al. (2006) and Mannucci et al. (2010) have additional systematic uncertainties associated with the validity of using the Kennicutt-Schmidt law to infer gas content, while direct gas measures must use an uncertain conversion between CO and H_2 mass. Combined with the broadly similar f_{gas} predictions among the models, this precludes any meaningful constraints as of yet from high- z gas fractions. The overall rate at which gas fractions go down with time at a given M_* is consistent with observations in all models (modulo at low masses at $z = 0$), suggesting that the basic physics governing gas fraction evolution has more to do with cosmological infall that is same among all models as argued in §4.3, as opposed to feedback mechanisms.

In summary, all simulations with outflows qualitatively reproduce the observed evolution of metallicity and gas fraction in galaxies. At a given M_* , all models produce rising metallicities and falling gas fractions with time. Quantitatively, the momentum-driven wind scalings model appears to be the best overall fit to the ensemble of observations. Nevertheless, significant discrepancies remain even in this case, particularly at the lowest and highest masses, which may owe systematic uncertainties in metal and gas measures, observational selection effects, and model deficiencies.

6 SCATTER & ITS SECOND PARAMETER DEPENDENCES

The small scatter in the mass-metallicity relation is a strong constraint on galactic chemical enrichment scenarios. While models have historically focused on reproducing the shape of the MZR, the reason for the small scatter, approximately 0.1 dex varying only mildly over more than 5 dex in stellar mass (Lee et al. 2006), remains unclear. Models invoking starburst-induced galactic outflows would predict larger scatter in lower-mass galaxies owing to the more stochastic nature of ejection from these systems.

As is evident from Figure 2, the situation in simulations with outflows is more complex; for instance, our momentum-driven wind scalings model produces an MZR scatter at $z = 0$ that is in good agreement with data, and other models less so. Here we examine what governs the scatter in the MZR and $M_* - f_{\text{gas}}$ relations within the context of our equilibrium model, particularly focusing on second-parameter correlations of metallicity and gas fraction with star formation rate and environment.

6.1 Star formation rate

The mass-metallicity relation is observed to have second-parameter dependences (i.e. correlated scatter) with other galaxy properties. A particularly strong one that has been explored recently is the second-parameter dependence of MZR on star formation rate. Ellison et al. (2008) noticed

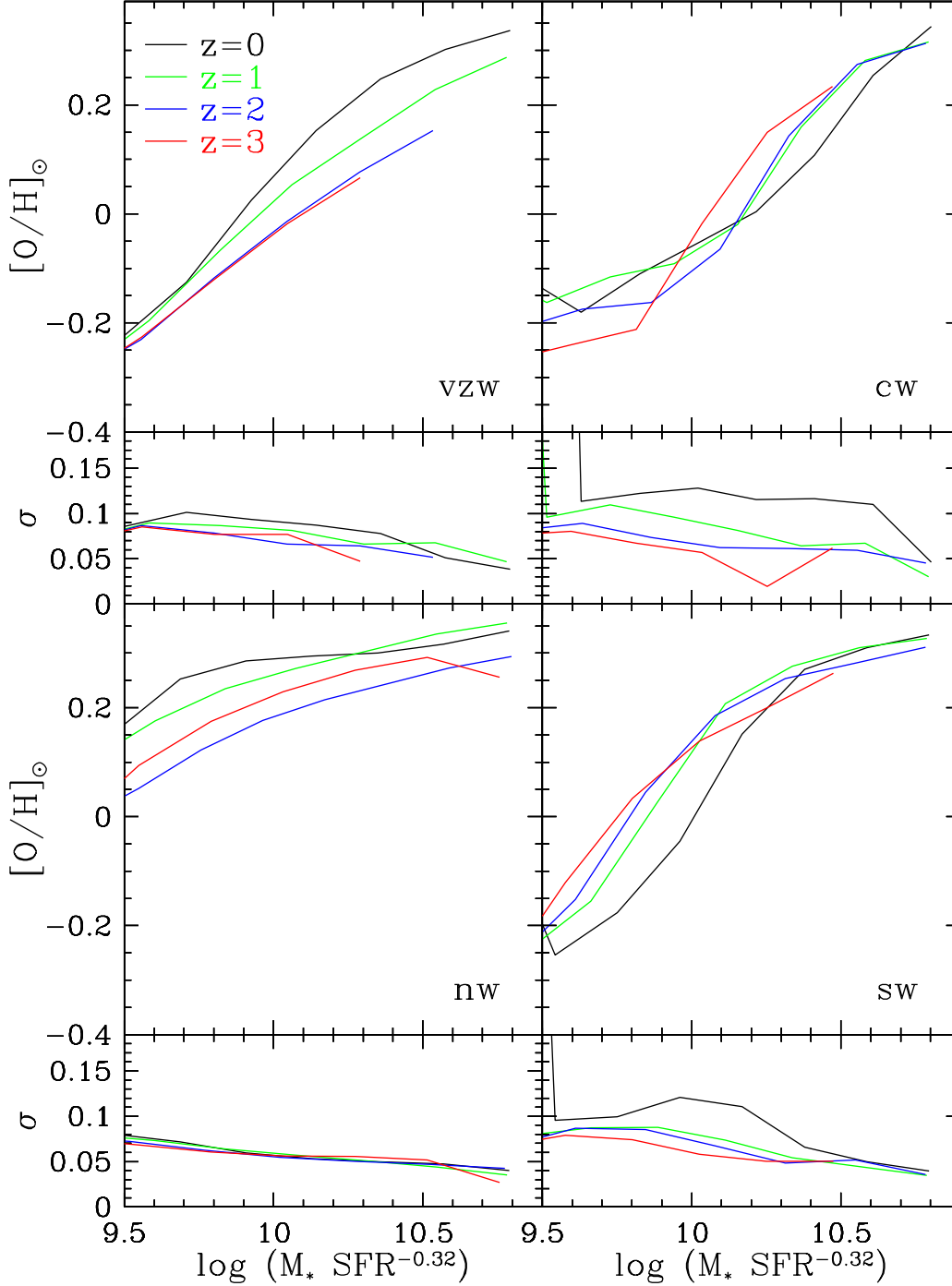


Figure 8. The fundamental metallicity relation, Z_{gas} vs. $M_* \text{SFR}^{0.32}$, in our r48n384 runs with four wind models at $z = 0, 1, 2, 3$. Lines with error bars show the running median. Small panels below each main panel show 1σ variance. The variance is smaller for the FMR as compared to the MZR (Figure 1). For comparison, observations of the FMR by Mannucci et al. (2010) found a variance of $\sigma = 0.053$.

that galaxies with higher star formation rates tend to lie below the mean MZR. Mannucci et al. (2010) developed this idea further, and noted that a specific combination of M_* and SFR, which they called the fundamental metallicity relation (FMR), led to a significantly smaller scatter. Furthermore, this relation appears to be invariant in redshift out to $z \sim 2.5$. Hence the relation between mass, metallicity, and SFR provides an even more stringent test of model predictions.

Figure 1 shows galaxies color-coded by star formation rate into high (blue), medium (green), and low (red) SFR relative to the mean within each stellar mass bin. It is a generic result from all simulations that high SFR galaxies tend to lie below the mean MZR, and low SFR systems lie above. Hence the observed second-parameter trend of the MZR on SFR is naturally reproduced in all simulations. This suggests a fundamental process at work, independent of feedback, that yields this trend. We will now argue that it

is a natural outcome of the equilibrium model for the MZR discussed in §3.1.

According to the equilibrium model, a galaxy of a given mass prefers to be at an equilibrium metallicity that is established by its current mass loading factor (Equation 7), which sets the amount of enrichment relative to fresh infall. When perturbed from its equilibrium metallicity owing to, say, a merger, this increases the galaxy mass while lowering the metallicity (since smaller galaxies have lower metallicities). This moves the system below the mean MZR. Concurrently, it results in a more gas-rich galaxy (i.e. a high outlier in $M_* - f_{\text{gas}}$), which in turn stimulates star formation. This correlated behavior is the origin of the trend that high-SFR galaxies lie at lower metallicity.

Conversely, a galaxy that suffers a lull in accretion will consume its gas into stars and form more metals, enriching itself along the locus of $Z \propto M_*$ (when the metallicity is significantly below the true yield). This is steeper than the MZR slope, and thereby the galaxy moves above the mean MZR. Once accretion restarts, the metals become diluted, and the galaxy is able to return to the equilibrium relation. In some cases, the galaxy is a small satellite dwarf that is being environmentally quenched, and it will never restart accretion. In the case the system can end up quite far above the MZR, as observations by Peeples, Pogge, & Stanek (2008) illustrate.

From the discussion above it is clear that this scenario will yield second parameter trends of gas fraction with SFR as well. As seen in Figure 3, galaxies with higher SFRs at a given mass tend to have high gas fractions. Such galaxies are undergoing an enhanced rate of star formation relative to a typical galaxy along the M_* -SFR relation, and hence will soon consume the gas and return to the mean relation. In this way, galaxies wobble around the mean MZR, $M_* - f_{\text{gas}}$, and main sequence relations owing to fluctuations in accretion. Deviations from equilibrium tend to return a galaxy to equilibrium, which is why this scenario is dubbed the “equilibrium model.” While outflows govern the overall shape and amplitude of these relation, the qualitative second-parameter trend with SFR is not a consequence of outflows, but rather of equilibrium. This is why the no-wind model shows the same second-parameter trend as the wind models.

Outflows do, however, play a significant role in quantitatively establishing the amount of scatter of the MZR and MGR. A consequence of the equilibrium model, as emphasized in Finlator & Davé (2008), is that the amount of scatter reflects how fast a galaxy can return to equilibrium after it suffers a perturbative event. To do so, there must be sufficient infall to re-equilibrate the galaxy. This can be quantified by the dilution time (Finlator & Davé 2008),

$$t_{\text{dil}} \equiv \frac{M_{\text{gas}}}{\dot{M}_{\text{in}}} = (1 + \eta)^{-1} \frac{M_{\text{gas}}}{\dot{M}_*} = (1 + \eta)^{-1} t_{\text{dep}}, \quad (10)$$

where we have used Equation 6 and the definition of t_{dep} (eq. 8). So long as $t_{\text{dil}} \lesssim t_{\text{vir}}$, where t_{vir} is the dynamical time at the halo virial radius, the scatter about the equilibrium relation will be small (Finlator & Davé 2008). As shown in Figure 4, t_{dep} becomes larger at smaller masses. If $\eta = \text{constant}$ as in our cw and sw simulations, the scatter will eventually rise significantly at low masses when the dilution time becomes longer than the virial time. This can

be seen at the lowest masses in the right panels (cw and sw) of Figure 2. Conversely, in our momentum-driven wind scalings case, the trend of η with M_* mitigates the increase in t_{dep} to low masses, and keeps the scatter small at smaller masses. Specifically, the vzw model (similar to all models) yields $t_{\text{dep}} \propto M_*^{-0.3}$, which at $\eta \gg 1$ (small masses) is almost exactly cancelled by $\eta \propto M_*^{-1/3}$ in this model. So one still expects the dilution time, and hence the scatter, to be constant to low masses. Observations by Lee et al. (2006) indicate a fairly constant scatter to low masses, though selection effects may be artificially lowering this (H. J. Zahid, priv. comm.). In any case, the scatter in these relations provides an independent avenue to constrain $\eta(M_*)$.

We now examine more quantitatively the second-parameter dependence of the MZR on SFR. Figure 8 shows the FMR for our simulated galaxies, namely gas-phase oxygen abundance versus $M_* \text{SFR}^{-0.32}$ (Mannucci et al. 2010), with the scatter indicated in the smaller panels below each main panel. As can be anticipated from Figure 1, the scatter is lowered using this combination for the x -axis. It is not as low as observed ($\sigma = 0.053$ dex), but a somewhat different combination of M_* and SFR can lower the model scatter further.

Furthermore, the simulated FMR shows significantly less evolution from $z = 3 \rightarrow 0$ than the MZR (note that the y -axis scale is significantly smaller than in Figure 2). At $z > 3$, Mannucci et al. (2010) observes the FMR to evolve strongly, which is a consequence of the low observed metallicities in $z > 3$ galaxies (see Figure 7), but observations by Richard et al. (2011) indicate no evolution out to $z \sim 3$. The lack of evolution has been taken to indicate that the FMR has a special significance that transcends cosmic epoch. In our models, however, the lack of (or slow) evolution in the FMR is mostly a coincidence; it just so happens that the increase in metallicity from high- z to low- z is balanced by the evolution in typical star formation rates for that particular combination of parameters. The fundamental principle that drives the FMR at any given epoch, namely the tendency for galaxies to be drawn towards an equilibrium MZR, has little to do with the overall evolution of the SFR at a given mass, which is set by cosmic inflow (e.g. Paper I).

Other observations have noted lower metallicities in merging systems. Ellison et al. (2008b) showed that close pairs tend to have a lower metallicity for their mass. It is possible that this trend is driven by the increase in SFR in these systems as driven by the interaction, although the lack of resolution in our models precludes us from examining this directly. Peeples, Pogge, & Stanek (2009) similarly found that strong outliers below the MZR tend to be interacting galaxies and are often quite massive. Once again this could be related to their SFR, although massive interacting galaxies often have significant AGN activity that produces a harder radiation field within their ISM, which when using abundance ratios to measure abundances can mimic a lower metallicity (C. Tremonti, priv. comm.). While these trends are interesting, it is unclear whether they are distinct from the overall trend of lower metallicities in higher SFR galaxies (at a given M_*). Finally, we mention that Ellison et al. (2008) found that systems with large half-light radii, like with high SFR, also lie below the mean MZR. Unfortunately, our simulations lack sufficient resolution to

robustly model galaxy sizes, so we cannot directly examine this second-parameter dependence.

The scatter in f_{gas} should, according to this scenario, follow the same trend as for the metallicity. Figure 6 shows that in the compilation of Peeples & Shankar (2010), the scatter is lower at small masses. This may be partly a selection effect, since particularly at small masses H I or CO selected samples will pick out the most gas-rich systems, artificially lowering the scatter. In the stellar mass-selected GASS sample of Catinella et al. (2010), there is no obvious evidence for a change in scatter in f_{gas} versus M_* among the galaxies that contain gas (excluding gas-poor passive systems), mirroring the roughly constant MZR scatter. In the context of the equilibrium model, this again argues for a mass loading factor that increases to lower masses.

In summary, galaxies in our simulations with high star formation rates at a given mass also have lower metallicities and higher gas fractions. This second-parameter dependence of the MZR and MGR is a natural and straightforwardly understood consequence of the equilibrium model. This dependence is independent of outflows, and arises purely as a consequence of equilibrium. Quantitatively, the dependence of scatter on M_* is a function of η and t_{dep} , and models that have larger mass loading factors at lower masses better match observations of constant or mildly increasing scatter in the MZR and MGR to the lowest masses. The FMR provides an interesting tool to quantitatively examine the second-parameter trend with SFR, and simulations yield broadly similar trends to those observed for the FMR.

6.2 Environment

Another second-parameter dependence of the MZR was noted by Cooper et al. (2008) and Ellison et al. (2008b), who showed that galaxies within dense environments such as groups and clusters tend to have higher metallicities. Galaxies outside such environments, in contrast, tend to have no obvious dependence on local galaxy density. This trend is over and above any trend associated with star formation. Our $48h^{-1}\text{Mpc}$ volume has some galaxy groups up to virial masses of $\sim 10^{14}M_{\odot}$, but not enough to compare directly to observations of clusters. However, we can examine the trend in metallicity with environment as measured by local galaxy density.

Figure 9 shows the $z = 0$ MZR for our four wind models, where we have subdivided galaxies by local galaxy density as measured in a $1h^{-1}\text{Mpc}$ tophat sphere. Galaxies at densities $> 0.5\sigma$ above the mean are shown in red, $< 0.5\sigma$ below the mean in blue, and those in between in green. A running median for the MZR, with 1σ variance, is shown for each sub-population.

The momentum-driven scalings and no-wind cases display the observed trend: Galaxies in high-density regions lie above the mean MZR by ~ 0.05 dex, while galaxies in medium and low density regions show no discernible difference. The constant- η models show significantly less dependence on environment. The differences disappear at the most massive end in all models.

One reason for this dependence may be that denser environments have more enriched intergalactic gas (e.g. Oppenheimer & Davé 2006), so accretion onto galaxies in those environs is likely to boost the metallicity over galaxies

in a less dense region. We believe this is indeed the trend responsible, but how this operates is subtle, and gives rise to distinct features among the wind models.

The model trends are best understood if the metallicity of infalling gas is governed by wind recycling. Recall that the IGM is almost entirely enriched by winds (e.g. Oppenheimer & Davé 2006), and so any metals falling back into galaxies constitutes wind recycling. At high masses, wind recycling is so effective that all galaxies re-accrete their ejected material quickly (Oppenheimer et al. 2010), which is like having no winds at all, so the metallicity approaches the overall yield regardless of environment (modulo an increase due to enriched infall; see §7). At sufficiently low masses, all ejected material escapes, and hence the infalling material is mostly primordial regardless of environment. But in the intermediate regime, environment plays a critical role in slowing winds (Oppenheimer & Davé 2008), in the sense that denser regions slow winds more and cause faster recycling.

As shown in Oppenheimer et al. (2010), in the case of momentum-driven scalings this intermediate regime occurs over a protracted range in M_* since $v_w \propto v_{\text{esc}}$; this protracted mass range is reflected in this model's dependence of MZR on environment. In the constant- v_w cases (cw and sw), there is only a small range of masses between the fully-escaping and fully-recaptured regimes (around the mass where $v_w \approx v_{\text{esc}}$), which means that the environmental dependence is only seen over ~ 0.5 dex in mass. Hence in these models, the high-density MZR actually shows a peak in metallicity at the mass where recycling is most effective. It occurs at higher M_* in the cw case relative to sw since its higher wind speed allows escape up to larger galaxies.

Empirically in our simulations, the dependence of metallicity on environment seems to be only effective when the environment becomes quite dense; medium and low density regions show no difference. This is likely because only these dense environments have hot gaseous halos (Kereš et al. 2009a) that can significantly slow winds. The no-wind case also shows a dependence on environment that is obviously not driven by wind recycling, but may be driven by tidal stripping (and subsequent enriched infall) which is more effective in dense regions; indeed, in §7 we show that the no-wind case at $z = 0$ has non-negligibly enriched infall. We leave a more detailed study of these effects for the future. Here we simply suggest that the environmental dependence of wind recycling governs how local galaxy density impacts the MZR, and our momentum-driven wind scalings model generally reproduces the observed trend. If this is true, studying the environmental dependence of the MZR offers a unique probe into cycle of baryons in and out of galaxies.

6.3 Satellites

Satellite galaxies are seen to have higher metallicities at a given stellar mass (Peeples, Pogge, & Stanek 2009). The origin of this trend is qualitatively understood within the equilibrium model: Satellites tend to live in dense regions where the infalling gas is more enriched, and furthermore they are not straightforwardly fed by cold streams since they do not lie at the bottom of the halo's potential well and hence evolve upwards off the MZR. In this section we quantitatively assess

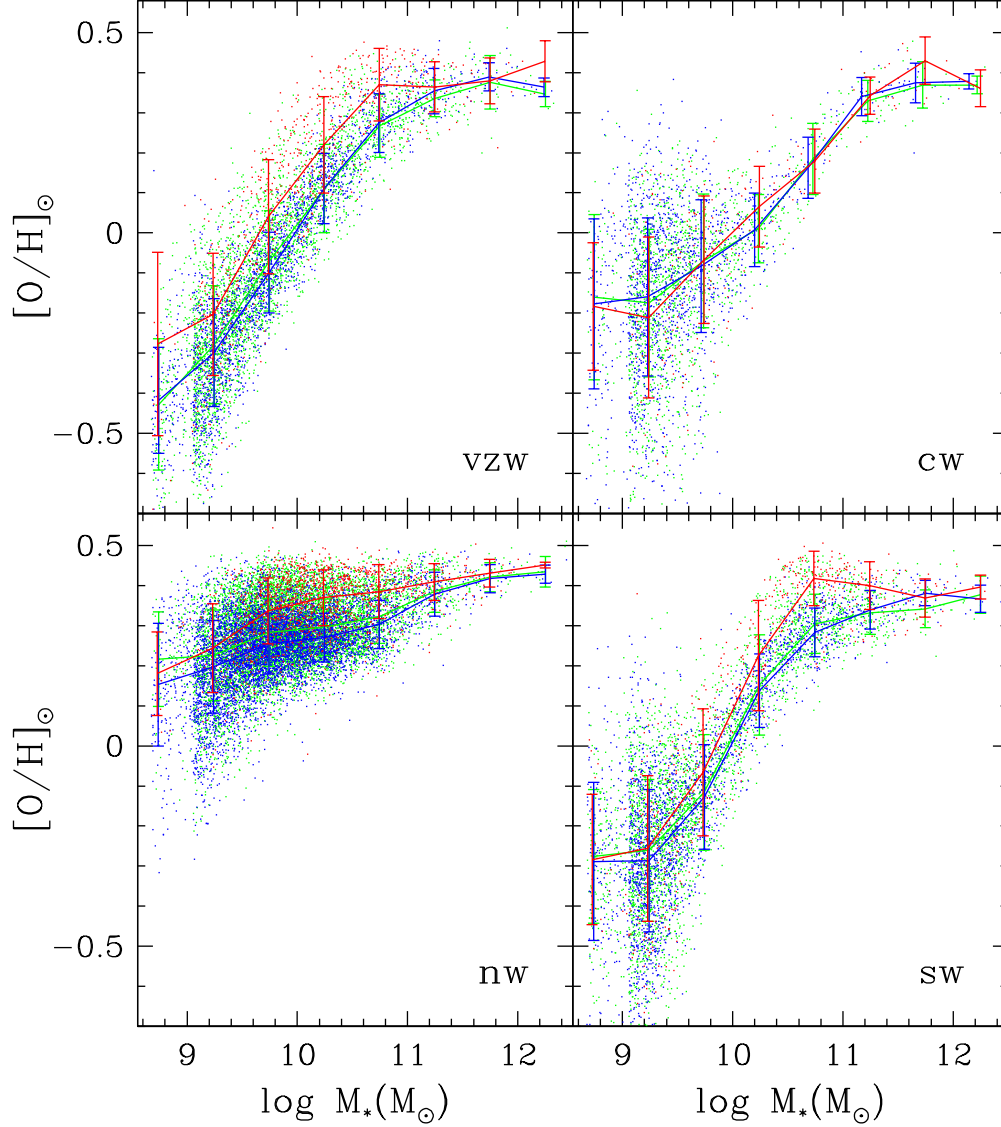


Figure 9. MZR at $z = 0$ in our four wind models subdivided by environment (i.e. local galaxy density in a $1h^{-1}\text{Mpc}$ sphere): High density ($> 0.5\sigma$ above average; red), low density ($> 0.5\sigma$ below average; blue), and middle (within 0.5σ of average; green).

the differences in satellite versus central populations for the various second-parameter trends we have examined above.

Figure 10 shows the median mass-metallicity relations for a variety of second-parameter dependences. In order to more easily see the dependences, we have subtracted out the overall MZR from each subsample’s MZR. The plot shows $\Delta[\text{O}/\text{H}]_{\odot}$ dependences on three variables: Star formation rate, environment, and satellite vs. central galaxies. For the first two quantities, we subdivide the overall sample into “high” and “low”, which simply means above and below the median within each mass bin. In the left panels, we show the median (differenced) MZR for galaxies with high-SFR as blue, and low-SFR as red. In the right panels, we analogously show the MZR for high-density environment galaxies in red, and low in blue. Top panels show the vzw simulation, and bottom panels show the no-wind run.

We further explore the dependence of SFR and environment within satellite (dotted lines) and central (dashed)

galaxy samples. This is done for the full sample (black), high-SFR/low-density (blue) and low-SFR/high density (red). The solid line at 0 represents the original MZR of all galaxies. In all, this figure shows how the dependences on SFR and environment interplay with the distinction between central and satellite galaxies.

Let us begin examining Figure 10 by considering the blue and red solid curves, i.e. the MZR subdivided by SFR and environment. These trends have been noted earlier, but here the differences are more visible since we have subtracted off the overall trend. Comparing the solid red and black curves, we see that, as before, low-SFR and high-environment galaxies lie above the global MZR, at least for galaxies with $M_* \lesssim 10^{11} M_{\odot}$. The trend with environment is generally stronger than the trend with SFR, which may be surprising given that this second-parameter dependence has received less attention in the literature. In the context of the equilibrium model, this indicates that denser envi-

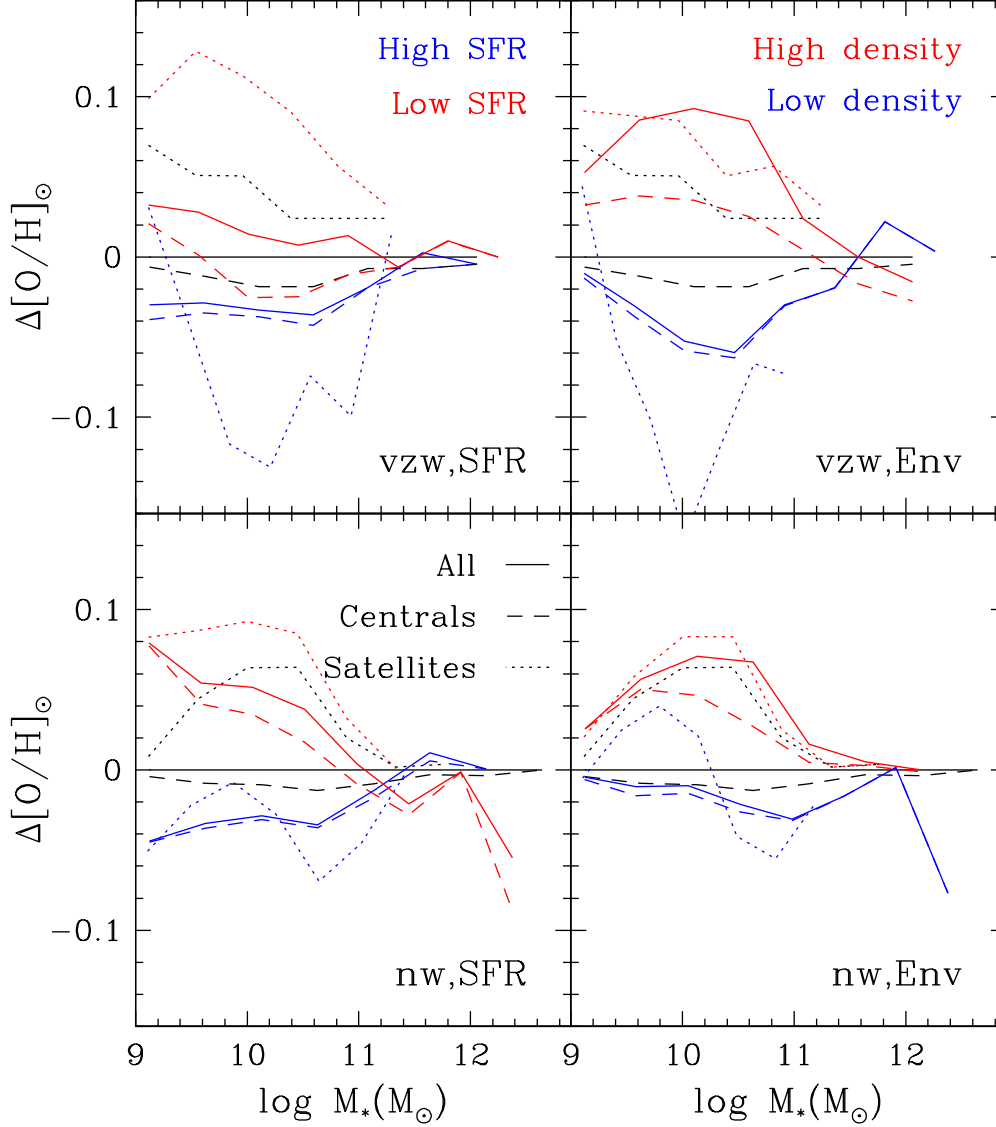


Figure 10. Second-parameter dependences of the MZR subdivided by satellite vs. central galaxies at $z = 0$ in our simulations. Each curve shows the *difference* between the MZR for a particular subsample of galaxies; the solid black curve at zero shows the overall MZR for that model. Top panels show the momentum-driven wind scalings case, bottom panels the no-wind simulation. Left panels show galaxies subdivided by star formation rate (at a given mass) above and below the mean. Right panels show galaxies analogously subdivided by environment. The blue curves show galaxies with above-median SFRs (in left panels) and below-median environments (right panels), red curves show below-median SFRs and above-median environments. Dashed and dotted black curves show the MZR for satellites and centrals, respectively. These populations are further subdivided into high-SFR/low-environment (dashed and dotted blue curves) and low-SFR/high-environment (dashed and dotted red curves).

ronments result in significant suppression and enrichment of inflow, such that galaxies within dense regions both have lower star formation rates (causing higher metallicities) and are accreting higher metallicity gas.

The source of these trends is further clarified when examining the satellite galaxy population. Overall, satellite galaxies (dotted curves) show elevated metallicities at a given mass compared to central galaxies (dashed curves), mimicking observed trends (Peeples, Pogge, & Stanek 2009). Since satellites have typically lower SFRs (Paper I) and also tend to live in denser environments, both second-parameter dependences discussed previously could be contributing the satellites' higher MZR. A particularly

striking result is that the second-parameter dependence on SFR is fairly small in the central galaxies, and is dominated by the satellite systems. That is, there is an enormous difference between the metallicities of high-SFR satellites (dotted blue) versus low-SFR satellites (dotted red) over most of the sub- M^* mass range. The trend is very strong in the vzw run, but also present in the nw run. The detailed physical origin of this we leave for future work, but here we speculate that galaxies first entering another halo will have enhanced SFR due to interactions and therefore will have lower metallicities, but will then get quenched and quickly build up metallicity to go above the mean MZR. In any case, it is evident that in these simulations, the

second-parameter dependence of the MZR on SFR is driven more by the satellite galaxies, while centrals show only a modest such dependence.

Looking at satellites vs. centrals subdivided by environment, it is not as clear here what is driving the overall trend. Both centrals and satellites show higher metallicities in dense regions. In the vzw model, the trend is somewhat stronger for satellites, but not as dramatically as in the case of SFR. Satellites are affected by both diminished (from strangulation) and enriched inflow, while central galaxies should not have inflow enriched, only diminished since they should still accrete gas normally at the bottom of the halo's potential well regardless of environment. That the strength of the effect is only slightly stronger for satellites indicates that the majority of the change to the MZR in dense regions arises because inflow is more enriched owing to residing in a denser region. It is worth noting that these changes in metallicity are, in an absolute sense, not large: they are typically below 0.1 dex. Therefore even a modest metallicity-density gradient in the IGM (Oppenheimer et al. 2011) could preferentially cause galaxies in denser environments to be over-enriched by this amount.

In summary, both environment and star formation rate play an important role in driving second-parameter trends in the MZR. The majority of this trend is driven by satellite galaxies, as central galaxies are less affected by these second parameter trends. This shows, as expected, that satellites have greater fluctuations in their accretion rates that drive star formation, and are more impacted by environmental effects. The overall trends are consistent with expectations from the equilibrium model, being driven by a competition between recent accretion and outflows. In the case of satellites vs. centrals at a given stellar mass, the outflow rates are similar in the simulations (being zero in the no-wind case), but the accretion rates can vary owing to both general stochastic fluctuations and environmental suppression. The typical difference in metallicities between satellites and centrals is quite small, typically of order 0.1 dex, so particular care is needed to tease out such effects in observed samples.

7 EVOLUTION IN GAS & METAL CONTENT

We have previously studied the evolution of the overall MZR and MGR relations, finding that at a given mass, metallicities rise slowly and gas fractions fall slowly with time. In this section we examine in more detail how particular galaxies evolve within these relations, in order to better understand the nature of the overall evolution.

Figure 11 shows galaxy tracks in MZR space (top panel) and MGR space (bottom panel) from $z = 2 \rightarrow 0$. We choose our vzw model since it does the best job of matching observations (with notable exceptions) of the models considered. To make these tracks, three representative stellar masses were selected at $z = 0$ (specifically $10^{12.13}$, $10^{10.57}$, $10^{9.85} M_\odot$), and 20 galaxies were chosen closest to each mass. The main progenitors of each galaxy were identified in each output back to $z = 2$, where the main progenitor is the galaxy at an earlier epoch hosting the largest fraction of the final galaxy's particles. The tracks shown are the mean value of the 20

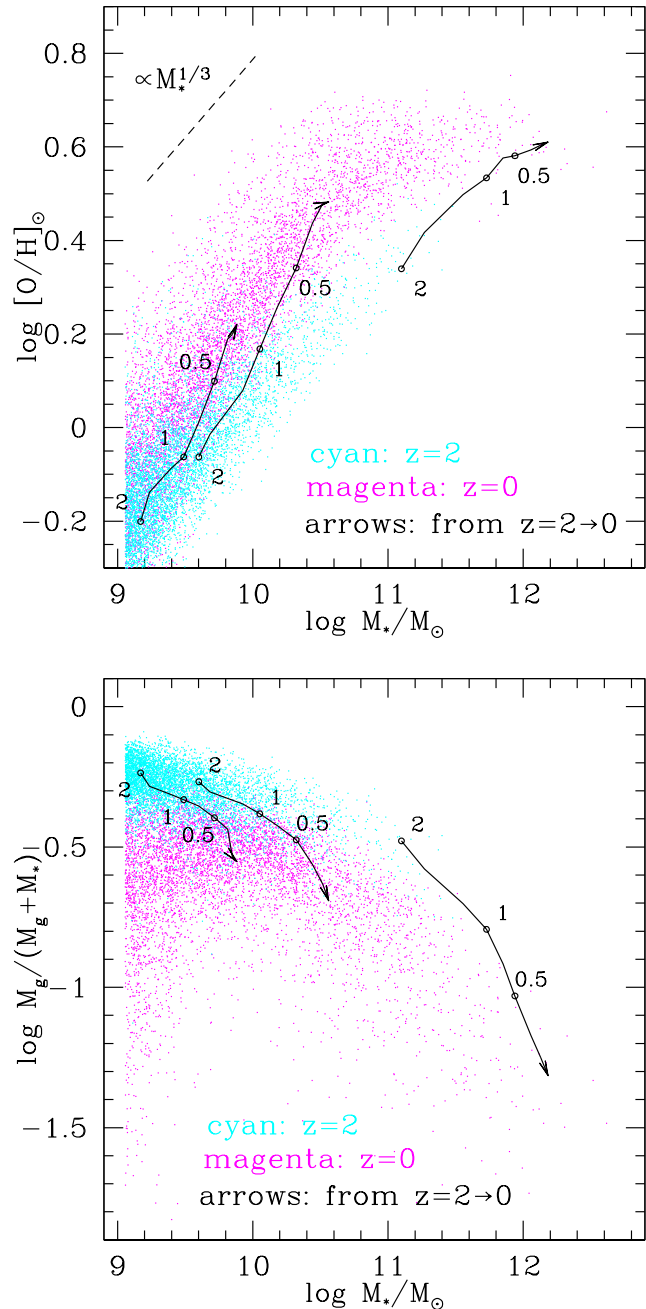


Figure 11. Evolution from $z = 2 \rightarrow 0$ of mean metallicity (top panel) and gas fraction (bottom) versus stellar mass for a set of galaxies within 3 mass bins in our r48n384vzw run. Cyan and magenta points show the overall galaxy population at $z = 2, 0$, respectively. Numbers along the tracks indicate the redshift; tracks end at $z = 0$.

progenitors. Numbers along the tracks indicate the redshift, with the tracks ending in an arrow at $z = 0$.

The most evident trend is that galaxies tend to evolve mostly *along* the mean MZR and MGR relations, as noted by Brooks et al. (2007) for the MZR. This directly translates into a slow evolution for these relations. The fact that galaxies move along these relations has sometimes been forwarded as the “cause” for the slow evolution, but this merely

begs the question, why do galaxies tend to move along these relations?

To answer this, let us first consider the MZR. It is straightforward to differentiate Equation 7 to show that if $\eta \propto M_*^{-x}$, then $d \log Z / d \log M_* = x$ when $\eta \gg 1$; this is the equilibrium model prediction for the slope of the galaxy track in MZR space at low masses, assuming that the constant of proportionality for η for a given galaxy is unevolving³. Hence if a galaxy obeys Equation 7 at all times, it will evolve directly along the MZR relation when $\eta \gg 1$. For example in the vzw case, $x = 1/3$, which is identical to the MZR slope in the low- M_* regime.

However, Figure 11 shows that the evolutionary slope is steeper than this: for the lower mass bins, $d \log Z / d \log M_* \approx 0.6$. The more rapid evolution must arise because an assumption in Equation 7 is violated. In particular, it turns out that the infall is not pristine as assumed in that equation. Oppenheimer et al. (2011, Figure 3) shows that the metallicity just outside star-forming regions (i.e. at $n_H \approx 0.13 \text{ cm}^{-3}$) rises substantially from $z = 2 \rightarrow 0$, and exceeds solar today. They argue that this arises owing to the preponderance of recycled wind accretion at later epochs, which causes the inflow from the IGM to be increasingly enriched.

Following Finlator & Davé (2008), we can extend Equation 7 to include the effects of enriched infall. If we define α_Z as the ratio of infalling gas metallicity (Z_{infall}) to the metallicity within the ISM of the galaxy (Z_{ISM}), then

$$Z = \frac{y}{1 + \eta} \frac{1}{1 - \alpha_Z}. \quad (11)$$

We can directly measure α_Z in our simulations. For a given mass, we take 50 galaxies near that mass and compute the mean metallicity within the ISM (i.e. star-forming) gas. We then compute the mean metallicity in infalling gas. We define infalling gas as all gas within 30 kpc (comoving) that is *not* star-forming and is moving towards the galaxy (i.e. $\mathbf{v} \cdot \mathbf{r} < 0$). We also tried scaling the infall radius with the virial radius at different masses, with only minor differences.

The evolution of Z_{ISM} and Z_{infall} are shown as the solid and dotted lines in the top panel of Figure 12. We show the vzw model at two masses, and the no-wind case at $M_* \approx 10^{10} M_\odot$. The metallicity is higher around larger galaxies, as expected. The interesting trend is that Z_{infall} increases faster than Z_{ISM} . This is quantified in the bottom panel where we plot $(1 - \alpha_Z)^{-1}$, which is the extra factor in Equation 11 accounting for enriched infall. The key point is that, from $z = 2 \rightarrow 0$, this term increases by 0.2 – 0.3 dex. This is identical to the excess increase in the galaxy metallicity above simply moving up along the MZR (Figure 11). The perhaps surprising implication is that the rising metallicity at a given stellar mass is not the result of galaxies processing more gas into stars, but rather the result of an increasing metallicity in accreted gas.

The no-wind case also shows a similar increase in $(1 - \alpha_Z)^{-1}$ of about 0.2 dex from $z = 2 \rightarrow 0$. In this

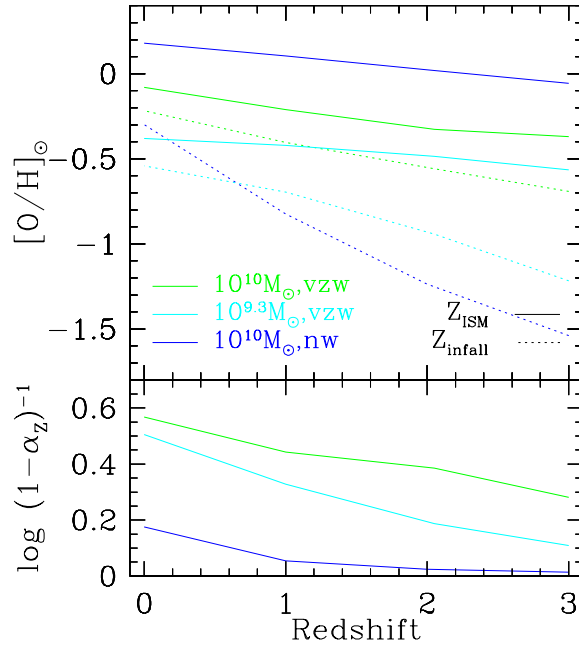


Figure 12. Top panel shows the evolution from $z = 3 \rightarrow 0$ of metallicity in the ISM Z_{ISM} (solid lines) and metallicity of infalling gas Z_{infall} (dotted lines). Infalling gas is all gas within 30 comoving kpc that is not star-forming and is moving towards the galaxy. Green and cyan curves show results for the vzw simulation at stellar masses of 2×10^9 and $10^{10} M_\odot$, respectively. The blue curves show the results for the no-wind case at $10^{10} M_\odot$. Bottom panel shows the extra multiplicative term in the equilibrium model MZR (Equation 11) that accounts for enriched infall, namely $(1 - \alpha_Z)^{-1}$ where $\alpha_Z \equiv Z_{\text{infall}}/Z_{\text{ISM}}$. This shows that enriched infall is primarily responsible for the upward evolution of the MZR in our simulations.

case, this arises because tidal interactions distribute metals around galaxies that can later fall back in. This only because prominent since $z \sim 1$. Overall, the enriched infall term is much lower than in the vzw case, showing that most of the enrichment in the infall is generated by outflows.

The gas fractions of our selected galaxies also show an evolution generally along the relation. The evolution does become notably steeper at low redshifts ($z \lesssim 0.5 - 1$) and at small masses, which shows that the “turnover” in low- M_* gas fractions is a late-time phenomenon. These dwarf galaxies are apparently depleting their gas reservoir too quickly, and are prevented from re-acquiring their ejected material owing to preventive feedback processes. We leave a fuller examination of the interplay between such feedback processes and gas content in dwarf galaxies for the future.

In summary, the slow evolution of the MZR and MGR scaling relations procedurally arises from the fact that galaxies tend to evolve mostly along these relations, with only mild deviations towards higher metallicity and lower gas fractions with time. Within the equilibrium model, the higher metallicities arise because gas infall is increasingly enriched to lower redshifts, while the lower gas fractions arise because the depletion time becomes smaller compared to the star formation timescale. While these trends are qualitatively consistent with the idea that galaxies obtain a large reservoir and slowly consume their gas (while generating

³ This turns out to be basically true, although it is something of a coincidence: Equation 3 shows that for a given galaxy mass, σ drops with time, implying a higher η and thus a lower metallicity. However, this is countered by the fact that a given galaxy’s σ increases with time as it grows. It happens that the two effects mostly cancel out for any given galaxy.

metals), our simulations suggest that the actual physics is much more complex, driven by a balance between inflow and outflow processes.

8 SUMMARY

In this paper and Paper I (Davé, Oppenheimer, & Finlator 2011) we have presented a study of how the stellar, gas, and metal contents of galaxies are governed by gas inflow and outflow processes within an evolving hierarchical Universe. In Paper I we investigated how galactic outflows play a key role in modulating the stellar growth of galaxies fed primarily by cold, filamentary accretion from the IGM. In this paper, we have shown that such inflow and outflow processes concurrently govern the evolution of the metallicity and gas fraction within star-forming galaxies.

The central message of these two papers is that the evolution of the main constituents of star-forming galaxies can be broadly understood within the context of a cycle of inflow and outflow between galaxies and the IGM. An idea that features prominently in our models for the evolution of the gas and metal content is the notion of equilibrium. Galaxies prefer to live on specific equilibrium relations between metal, gas, and stellar content, whose forms are set by the cosmologically-evolving inflow and outflow rates. The inflow rate into the ISM is tied to the accretion rate into halos, with notable departures at low masses and late epochs owing to preventive feedback. Meanwhile the outflow rate appears to be most closely tied to stellar mass, since e.g. the metallicity of a galaxy is observed to have the tightest correlation with its stellar mass as compared to any other individual property. Inflow fuels star formation, whereas outflows are the central governing agent that control how much of the inflowing material turns into stars. An key corollary of this scenario is that stochastic variations in the inflow rate tend to drive galaxies back towards the equilibrium relations, resulting in small scatters in metallicities and gas fractions that are correlated with star formation rate. This equilibrium paradigm can therefore quantitatively explain the origin of the shape, slope, and scatter of the relations between gas, metals, and stars, as arising naturally from hierarchical galaxy growth modulated by outflows.

With that framework in mind, we summarize the key conclusions of this paper:

- Galaxy metallicities are set by a balance between inflows that provides (relatively) pristine fuel, and outflows that reduce the cosmological star formation efficiency by ejecting fuel. This equilibrium can be expressed as a function of the outflow's effective mass loading factor η (eq. 7), meaning that the stellar mass-metallicity relation (MZR) mostly reflects the relationship between η and stellar mass.
- The evolution of the MZR in this scenario is expected to occur mostly along the relation, as confirmed by tracking simulated galaxies. In detail there is a slow upwards evolution in metallicity at a given stellar mass, i.e. the MZR rises with time. We demonstrate that this is quantitatively understood as a result of accreted gas becoming more enriched with time.
- Galaxy gas fractions reflect a competition between gas accretion, as quantified by the star formation timescale

(M_*/SFR), and gas consumption, as quantified by the depletion time ($M_{\text{gas}}/\text{SFR}$) (Equation 9). The depletion time in our models is set primarily by our assumed law for star formation (based on Kennicutt-Schmidt), while the star formation time is governed by cosmic inflow. Since both of these timescales are relatively insensitive to outflows, gas fractions are (in contrast to metallicities) likewise insensitive to outflows.

- The stellar mass-gas fraction relation (MGR) drops slowly with time in all models. This arises because the gas supply rate, driven by cosmic accretion, drops faster than the gas consumption rate, which is tied to the galaxy's dynamical time. Constant replenishment of ISM gas is a ubiquitous feature of these models, as appears to be required from observations. Galaxies individually evolve mostly along the MGR, but drop particularly at late epochs.

- Wind reaccretion plays an increasingly important role in the evolution of the MZR and MGR at late times, particularly at $z \lesssim 1$. Enriched inflow directly corresponds to material that was ejected at an earlier epoch, and alters the MZR (Equation 11). In the MGR, all wind models develop a turnover at late epochs and low masses, likely reflecting the lack of re-accretion of wind material in these systems.

- The scatter in the MZR and MGR reflects how fast a galaxy can return to equilibrium given a fluctuation in the accretion rate, as quantified by the dilution time given by $t_{\text{dep}}/(1 + \eta)$. The scaling of the MZR and MGR scatter with mass therefore provides an independent constraint on $\eta(M_*)$.

- Departures from equilibrium naturally correlate with star formation in all models, even without winds, as it is a consequence of equilibrium rather than feedback. Galaxies with high SFR for their M_* are predicted to have low metallicity and high f_{gas} , consistent with observations. Galaxies in denser regions and satellites are also predicted to have higher metallicities as observed, since these systems are obtaining more enriched inflow and/or their inflow has been curtailed because they are not residing at the center of the halo.

- Comparing to observations of the $z = 0$ MZR, the equilibrium model with momentum-driven wind scalings predicts an unbroken power law of $Z \propto M_*^{1/3}$ with small scatter as broadly observed, while the constant- η models predict a flattening of the MZR at low masses with a strongly increasing scatter. All models qualitatively reproduce the observed slow evolution of the MZR upwards from $z = 3 \rightarrow 0$, but the momentum-driven wind scalings model comes closest to matching data at both $z = 2$ and $z = 0$.

- Gas fractions at $z = 0$ in all wind models predict a falling f_{gas} with M_* at high masses, and a turnover to lower f_{gas} at the smallest masses. The former broadly agrees with data, while the latter is in clear disagreement with data. This turnover is related to a downturn in specific SFR and upturn in age in small systems (Paper I), and likewise may indicate that star formation in dwarfs must be delayed on cosmic timescales, perhaps owing to a different star formation law or less efficient conversion of HI to H₂ in these systems.

Taking a broader view, the problem of galaxy evolution appears to be separable into three phases, predominantly divided by halo mass, which could somewhat fancifully be called the birth phase, the growth phase, and the

death phase. In the birth phase, halos are small enough that photoionization plays a critical role in retarding accretion; these are galaxies below the so-called filtering mass (Gnedin 2000). In the growth phase, galaxy growth is regulated by baryon cycling, i.e. by smooth, filamentary accretion and ubiquitous outflows that circulate mass, energy, and metals between galaxies and the IGM. In the death phase, some mechanism (often associated with feedback from the central black hole) quenches accretion into the ISM, thereby halting star formation and creating a passive galaxy. Thus the three phases are not only distinct in halo mass but also have three separate dominant feedback mechanisms that govern galaxy growth, making galaxy evolution in each phase physically distinct from the others.

In this paper and Paper I we have focused on galaxies in the growth phase. In this phase, the dark matter halo virial radius as a boundary between the galaxy and the IGM is of secondary importance: gas flows in and out unabated through the virial radius. Major mergers are a sub-dominant fueling mechanism in such systems, and are relatively unimportant in the overall star formation history. Central black holes may be growing within these systems, but they play a minor role in the overall evolution. In contrast, the formation and evolution of passive “death phase” galaxies appears to be critically linked to major mergers, black holes with associated feedback, and the presence of a stable hot gaseous halo (e.g. Kereš et al. 2005) that demarcates the virialized region from the ambient IGM (e.g. Croton et al. 2006; Bower et al. 2006; Sijacki et al. 2007; Hopkins et al. 2008; Somerville et al. 2008; Di Matteo et al. 2008). The transition between the growth and death phases may be triggered by a major merger, such that bulge formation and black hole growth are linked (e.g. Hopkins et al. 2008), although it appears that maintaining a red and dead galaxy primarily relies on the existence of a hot gaseous halo (Croton et al. 2006; Gabor et al. 2011). While these phases are physically distinct, understanding the evolution of the galaxies in the death phase likely requires well-known “initial conditions” provided by galaxies in the growth phase.

Many key aspects of the galaxy life cycle are far from being fully understood. It will be a transformative achievement in the galaxy formation community when even the basic framework is in place, and that work can begin towards a quantitative rather than qualitative understanding of the main physical processes (analogous to the era of precision cosmology). In these two papers, we have illustrated how simulations can be used to elucidate simple analytic relationships between physical processes of inflow and outflow and the observable properties of galaxies. We have shown that cosmic dark matter-driven inflow combined with the mass loading factors, wind recycling properties, and preventive effects of outflows govern evolution of the basic constituents of galaxies. This provides a bridge between detailed studies of inflow and outflow, the latter being much more poorly understood, and large-scale surveys of galaxy properties across cosmic time. In other words, given a detailed model (e.g. from individual halo simulations) for outflow mass loading, wind recycling, and preventive effects, we can now translate that with good fidelity into predictions for the evolutionary properties of galaxy populations. Alternatively, it allows observations of galaxy populations to be straightforwardly interpreted as constraints on the detailed properties of inflows

and outflows. This scenario provides a first step towards understanding the much wider range of interesting observable galaxy properties, such as kinematics, radial gradients, morphologies, and environmental dependences. Continuing to grow the synergy between multi-scale models and multi-wavelength observations of galaxies and their surrounding gas is the best way to advance our understanding of the life cycle of galaxies across cosmic time.

ACKNOWLEDGEMENTS

The authors acknowledge A. Dekel, N. Katz, D. Kereš, J. Kollmeier, C. Papovich, J. Schaye, C. Tremonti, F. van de Voort, D. Weinberg, and H. J. Zahid for helpful discussions, and V. Springel for making GADGET-2 public. The simulations used here were run on University of Arizona’s SGI cluster, ice. This work was supported by the National Science Foundation under grant numbers AST-0847667 and AST-0907998. Computing resources were obtained through grant number DMS-0619881 from the National Science Foundation.

REFERENCES

- Arrigoni, M., Trager, S. C., Somerville, R. S., Gibson, B. K. 2010, *MNRAS*, 402, 173
- Asplund, M., Grevesse, N., Sauval, A. J., Scott, P. 2009, *ARA&A*, 47, 481
- Balogh, M. L., Pearce, F. R., Bower, R. G., Kay, S. T. 2001, *MNRAS*, 326, 1228
- Bower, R. G., Benson, A. J., Malbon, R., Helly, J. C., Frenk, C. S., Baugh, C. M., Cole, S., Lacey, C. G. 2006, *MNRAS*, 370, 645
- Brooks, A. M., Governato, F., Booth, C. M., Willman, B., Gardner, J. P., Wadsley, J., Stinson, G., Quinn, T. 2007, *ApJL*, 655, L17
- Catinella, B. et al. 2010, *MNRAS*, 403, 683
- Chabrier G., 2003, *PASP*, 115, 763
- Chieffi, A. & Limongi, M. 2004, *ApJ*, 608, 405
- Cooper, M. C., Tremonti, C. A., Newman, J. A., Zabludoff, A. I. 2008, *MNRAS*, 390, 245
- Croton, D. J. et al. 2006, *MNRAS*, 365, 11
- Daddi, E. et al. 2007, *ApJ*, 670, 156
- Dalla Vecchia, C., Schaye, J. 2008, *MNRAS*, 387, 1431
- Davé, R. et al. 2001, *ApJ*, 552, 473
- Davé, R., Finlator, K., Oppenheimer, B. D. 2006, *MNRAS*, 370, 273
- Davé, R. 2008, *MNRAS*, 385, 147
- Davé, R., Oppenheimer, B. D., Finlator, K. M. 2011, *MNRAS*, submitted
- Dekel, A. & Silk, J. 1986, *ApJ*, 303, 39
- Dekel, A. & Woo, J. 2003, *MNRAS*, 344, 1131
- Dekel, A. et al. 2009, *Nature*, 457, 451
- Di Matteo, T., Colberg, J., Springel, V., Hernquist, L., Sijacki, D. 2008, *ApJ*, 676, 33
- Eggen, O. J., Lynden-Bell, D., Sandage, A. R. 1962, *ApJ*, 136, 748
- Elbaz, D. et al. 2007, *A&A*, 468, 33
- Ellison, S. L., Patton, D. R., Simard, L., McConnachie, A. W. 2008, *ApJL*, 672, L107

- Ellison, S. L., Patton, D. R., Simard, L., McConnachie, A. W. 2008b, *AJ*, 135, 1877
- Erb, D. K., Shapley, A. E., Pettini, M., Steidel, C. C., Reddy, N. A., Adelberger, K. L. 2006, *ApJ*, 644, 813
- Erb, D. K., Steidel, C. C., Shapley, A. E., Pettini, M., Reddy, N. A., Adelberger, K. L. 2006, *ApJ*, 646, 107
- Faucher-Giguere, C. A., Kereš, D., Ma, C.-P. 2011, *MNRAS*, submitted, arXiv:1103.0001
- Finlator, K., Davé, R., Papovich, C., Hernquist, L. 2006, *ApJ*, 639, 672
- Finlator, K. & Davé, R. 2008, *MNRAS*, 385, 2181
- Gabor, J. M., Davé, R., Finlator, K., Oppenheimer, B. D. 2010, *MNRAS*, in press
- Gabor, J. M., Davé, R., Finlator, K., Oppenheimer, B. D. 2011, in preparation
- Genzel, R. et al. 2010, *MNRAS*, in press
- Gnedin, N. Y. 2000, *ApJ*, 542, 535
- González, V., Labbé, I., Bouwens, R. J., Illingworth, G., Franx, M., Kriek, M., Brammer, G. B. 2010, *ApJ*, 713, 115
- Hinshaw, G. et al. 2009, *ApJS*, 180, 225
- Hopkins, P. F., Cox, T. J., Kereš, D., Hernquist, L. 2008, *ApJS*, 175, 390
- Katz, N., Weinberg, D. H., Hernquist, L. 1996, *ApJS*, 105, 19
- Kauffmann, G., et al. 2003, *MNRAS*, 341, 54
- Kennicutt, R. C. 1998, *ApJ*, 498, 541
- Kereš, D., Katz, N., Weinberg, D. H., & Davé, R. 2005, *MNRAS*, 363, 2
- Kereš, D., Katz, N., Fardal, M., Davé, R., Weinberg, D. H. 2009, *MNRAS*, 395, 160
- Kewley, L. J. & Ellison, S. L. 2008, *ApJ*, 681, 1183
- Köppen, J., Weidner, C., Kroupa, P. 2007, *MNRAS*, 375, 673
- Krumholz, M. R., Leroy, A. K., McKee, C. F. 2011, *ApJ*, in press
- Lee, H., Skillman, E. D., Cannon, J. M., Jackson, D. C., Gehrz, R. D., Polonski, E. F., Woodward, C. E. 2006, *ApJ*, 647, 970
- Mannucci, F., Cresci, G., Maiolino, R., Marconi, A., Gnerucci, A. 2010, *MNRAS*, submitted, arXiv:1005.0006
- Maraston, C., Pforr, J., Renzini, A., Daddi, E., Dickinson, M., Cimatti, A., Tonini, C. 2010, *MNRAS*, 407, 830
- McKee, C. F. & Ostriker, J. P. 1977, *ApJ*, 218, 148
- Mo, H. J., Mao, S., White, S. D. M. 1998, *MNRAS*, 295, 319
- Murray, N., Quatert, E., Thompson, T. A. 2005, *ApJ*, 618, 569
- Noeske, K. G. et al. 2007, *ApJL*, 660, L43
- Oppenheimer, B. D., Davé, R., Kereš, D., Katz, N., Kollmeier, J. A., Weinberg, D. H. 2010, *MNRAS*, 860, in press
- Oppenheimer, B. D. & Davé, R. 2006, *MNRAS*, 373, 1265
- Oppenheimer, B. D. & Davé, R. 2008, *MNRAS*, 387, 577
- Oppenheimer, B. D. & Davé, R. 2009, *MNRAS*, 395, 1875
- Oppenheimer, B. D., Davé, R., Finlator, K. 2009, *MNRAS*, 396, 729
- Oppenheimer, B. D., Davé, R., Katz, N., Kollmeier, J. A., Weinberg, D. H. 2011, in preparation
- Papovich, C., Finkelstein, S. L., Ferguson, H. C., Lotz, J. M., Giavalisco, M. 2010 *MNRAS*, submitted, arXiv:1007.4554
- Peeples, M. S., Pogge, R. W., Stanek, K. Z. 2008, *ApJ*, 685, 904
- Peeples, M. S., Pogge, R. W., Stanek, K. Z. 2009, *ApJ*, 695, 259
- Peeples, M. S., Shankar, F. 2010, *MNRAS*, submitted, arXiv:1007.3743
- Popping, A., Davé, R., Braun, R., Oppenheimer, B. D. 2009, *A&A*, 504, 15
- Rees, M. J., & Ostriker, J. P. 1977, *MNRAS*, 179, 541
- Richard, J., Jones, T., Ellis, R., Stark, D. P., Livermore, R., Swinbank, M. 2011, *MNRAS*, in press
- Robertson, B. E., Kravtsov, A. V. 2008, *ApJ*, 680, 1083
- Rupke, D. S., Veilleux, S., & Sanders, D. B. 2005, *ApJS*, 160, 115
- Salim, S. 2007, *ApJS*, 173, 267
- Savaglio, S. et al. 2005, *ApJ*, 635, 260
- Schmidt, M. 1959, *ApJ*, 129, 243
- Sijacki, D., Springel, V., Di Matteo, T., Hernquist, L. 2007, *MNRAS*, 380, 877
- Somerville, R. S., Hopkins, P. F., Cox, T. J., Robertson, B. E., Hernquist, L. 2008, *MNRAS*, 391, 481
- Springel, V. & Hernquist, L. 2003, *MNRAS*, 339, 289
- Springel, V. & Hernquist, L. 2003, *MNRAS*, 339, 312
- Springel, V. 2005, *MNRAS*, 364, 1105
- Steidel, C. C. et al. 2010, *ApJ*, 717, 298
- Tacconi, L. J. et al. 2010, *Nature*, 463, 781
- Tremonti, C. A. et al. 2004, *ApJ*, 613, 898
- van de Voort, F., Schaye, J., Booth, C. M., Haas, M. R., Dalla Vecchia, C. 2010, *MNRAS*, submitted, arXiv:1011.2491
- Weiner, B. J. et al. 2009, *ApJ*, 692, 187
- White, S. D. M., & Rees, M. J. 1978, *MNRAS*, 183, 341
- Zahid, H. J., Kewley, L. J., Bresolin, F. 2010, arXiv:1006.4877
- Zhang, D. & Thompson, T. A. 2010, *ApJ*, submitted, arXiv:1005.4691